INJECTION, TRANSPORT, AND IONIC INTERACTIONS OF CARRIERS IN POLYACETYLENE IONOMERS AS PROBED BY NEAR-INFRARED ABSORBANCE AND VISIBLE PHOTORESPONSE

by

ETHAN MICHAEL WALKER

A DISSERTATION

Presented to the Department of Chemistry and Biochemistry
and the Graduate School of the University of Oregon
in partial fulfillment of the requirements
for the degree of
Doctor of Philosophy

June 2015

DISSERTATION APPROVAL PAGE

Student: Ethan Michael Walker

Title: Injection, Transport, and Ionic Interactions of Carriers in Polyacetylene Ionomers as Probed by Near-Infrared Absorbance and Visible Photoresoponse

This dissertation has been accepted and approved in partial fulfillment of the requirements for the Doctor of Philosophy degree in the Department of Chemistry and Biochemistry by:

Catherine Page	Chairperson
Mark Lonergan	Advisor
James Hutchison	Core Member
Andrew Marcus	Core Member
Benjamin Aleman	Institutional Representative

and

Scott L. Pratt	Dean of the Graduate School

Original approval signatures are on file with the University of Oregon Graduate School.

Degree awarded June 2015

DISSERTATION ABSTRACT

Ethan Michael Walker

Doctor of Philosophy

Department of Chemistry and Biochemistry

June 2015

Title: Injection, Transport, and Ionic Interactions of Carriers in Polyacetylene Ionomers as Probed by Near-Infrared Absorbance and Visible Photoresoponse

While mixed ionic-electronic conductors (MIECs) show promise in a number of different device structures, their successful application has been inhibited by difficulties with characterization. The simultaneous influence of both ionic and electronic systems often foils attempts to quantify material parameters important for rational device design. In many cases, even general models of MIEC function can prove uncertain or controversial.

This dissertation addresses the broader issue of ambiguity in MIEC characterization by exploring near-infrared absorbance as a method of gaining further insight into these systems. In combination with a traditional suite of techniques, this method enables determination of parameters not otherwise accessible. The determination of a concentration-dependant carrier mobility in an MIEC material will be demonstrated, and MIEC conduction in the unipolar regime will be broadly described as a system of electrochemically-supported charge injection. This model will be subsequently expanded to describe an unusual and previously unreported phenomenon of rectification when MIECs are interfaced with otherwise appropriate semiconducting contacts. A model labeled as extracting-electrode space-

charge limited current will be described and experimentally demonstrated. Finally, the unique photovoltaic properties of an ionic heterojunction system comprising two MIECs will be examined. The results will be used to gain insight into the role of ionic asymmetry in the behavior of MIEC interfaces.

This dissertation contains coauthored, previously published, and unpublished work.

CURRICULUM VITAE

NAME OF AUTHOR: Ethan Michael Walker

GRADUATE AND UNDERGRADUATE SCHOOLS ATTENDED:

University of Oregon, Eugene
Fort Lewis College, Durango, CO

DEGREES AWARDED:

Doctor of Philosophy, Chemistry, 2015, University of Oregon
Bachelor of Science, Chemistry, 2006, Fort Lewis College

AREAS OF SPECIAL INTEREST:

Organic Electronics
Mixed Ionic-Electronic Conductors
Organic Photovoltaics

PROFESSIONAL EXPERIENCE:

Graduate Research Assistant, Department of Chemistry and Biochemistry, University of Oregon, Eugene, OR. 2007-2014

Graduate Teaching Assistant, Department of Chemistry and Biochemistry, University of Oregon, Eugene, OR. 2006-2007, 2014-2015

PUBLICATIONS:

Weber, C. D., Bradley, C., Walker, E. M., Robinson, S. G. & Lonergan, M. C. Increased Performance of Inverted Organic Photovoltaics Using a Cationically functionalized Fullerene Interfacial Layer. *Solar Energy Materials and Solar Cells* **129,** 90–94 (2014).

Walker, E. M. & Lonergan, M. C. Characterizing Charge Injection, Transport, and Mobility in a Conjugated Polyelectrolyte by NIR Absorbance. *J. Phys. Chem. C* 14929–14938 (2013).

Lin, F., Walker, E. M. & Lonergan, M. C. Photochemical Doping of an Adaptive Mix-Conducting p–n Junction. *J. Phys. Chem. Lett.* **1,** 720–723 (2010).

ACKNOWLEDGMENTS

I wish to thank first and foremost Mark Lonergan, who has provided guidance, practical experimental advice, prompt feedback, revealing discussion, understanding support, and no small measure of patience. Without his insight, both physical and personal, none of this work would have been possible. I would like to thank especially Fuding Lin and Yongjun Wang, whose revealing work on these systems provided the entire foundation for my own understanding. I would like to thank the other members of the lab in my time; David Stay, Iain Moody, Chris Weber, Don Clayton, and Colin Bradley, for assistance, feedback, and conversation, both helpful and diverting. Special thanks are owed to TJ Mills, whose previous work and helpful discussion made the analysis in Chapter II possible, and whose level of understanding I still aspire to. I would like to thank my friends, without whom I would have likely gone insane, and my family, for their unwavering support.

TABLE OF CONTENTS

Chapter Page

LIST OF FIGURES

Figure Page

Figure Page

CHAPTER I

GENERAL INTRODUCTION

1.1. Overview

The focus of this dissertation is the characterization of mixed ionic-electronic semiconductors (MIEC's). However, in a strongly application-driven research field such as this one, it is important to understand not only the physical characteristics of MIEC's, which will be discussed in the latter half of this chapter, but also the collection of prospective applications which frames this literature. The behavior of MIEC systems, and the applications to which they are applied, are almost always understood as a variation of an equivalent non-ionic organic semiconductor. Therefore, this discussion will begin by a background on organic semiconductors, and the device structures that ultimately guide MIEC research.

1.2. Organic Semiconductors: Background, Applications, and Relation to Inorganic Semiconductors

In 1977, Alan J. Heeger and Alan G. MacDiarmid published a paper which introduced the material science community to functionally doped organic semiconductors.[1] Using the conjugated polymer polyacetylene, they demonstrated that controlled doping could vary the conductivity over 11 orders of magnitude, ultimately reaching metallic levels of conduction. It was an exciting result that inspired expectations of a broad revolution in the field of semiconducting materials and devices.

Organic semiconductors possess a number of qualities that would recommend them over their inorganic counterparts. They can be considerably less expensive and energy intensive to produce than conventional semiconductors such as silicon, which must be heated over its (considerable) melting point in the course of processing. Soluble organic polymers and small-molecule semiconductors may also be processed by a variety of techniques[2] such as spin-coating, doctor-blading,[3] and ink-jet printing,[4] which enable fine control over the fabrication of thin conformal films, combined with good material economy. Small-molecule organic semiconductors are also often suitable to low-power thermal evaporation.[5] Organic semiconductors in general are also better suited to economic manufacturing methods such as roll-to-roll processing, and their flexibility enables a number of applications not possible with rigid crystalline semiconductors.[6] Organic

semiconductors only rely on earth-abundant elements, and likewise they rarely contain highly toxic or environmentally degrading elements which must be accounted for in disposal. Finally, organic chemistry allows for a degree of fine-tuning of material parameters not always available for inorganic materials based on a repeating crystal structure.

The potential advantages described above were largely apparent even in the early days of organic semiconductor research, so there was understandable optimism about the prospects for these materials. However, the early development, while scientifically interesting, rarely furnished revolutionary applications for the broader commercial and industrial world. While Heeger and MacDiarmid's 1977 paper[1] had shown a remarkably familiar behavior of polyacetylene in response to doping, as this rapidly expanding field of research progressed, it became more and more clear that there were deep distinctions between organic and inorganic semiconductors, not just in fabrication but in fundamental device physics. As a consequence, even while the field furnished exciting and unexpected physical and chemical insights, attempts to produce the "organic equivalent" of traditional semiconducting devices often yielded unimpressive results[7]. For example early organic photovoltaics, fabricated on the familiar model of existing solar cells, typically displayed power conversion efficiencies (PCE) below 0.1%.[8]

However in the last decade, organic semiconductor devices have emerged as commercially competitive alternatives in an increasing number of applications. Organic light-emitting diodes (OLED's) now light the displays of a number of high-

end electronic devices,[9] and the still-increasing efficiency of organic photovoltaics has risen high enough to be explored for commercial applications.[10] These and other applications have *not* been primarily enabled by more faithfully imitating the traditional semiconductors with which they compete. Rather, the maturing of this field is owed to an appreciation, and an increasingly comprehensive understanding, of the unique characteristics of organic semiconductors. These differences require alternate strategies to achieve familiar devices functions, but increasingly, they also suggest the development of entirely unanticipated applications.

Nowhere can the divergence of organic electronics from traditional semiconductors be seen more clearly than in the realm of photovoltaics. Traditional solar cells are constructed around P-N junctions, where carrier diffusion between disparately doped semiconductors results in depletion regions around the interface and the establishment of an electric field. When a photon strikes the semiconductor, it generates an exciton, which rapidly separates in the high-dielectric constant, high-mobility environment into a delocalized electron and hole. The interfacial electric field is such that the photogenerated minority carrier (opposite the sign of doping in the material) may be shepherded across the interface while the majority carrier is repelled. Thus a net photocurrent is established while the carriers retain the thermodynamic potential to do work through an external circuit (See Figure 1.1)

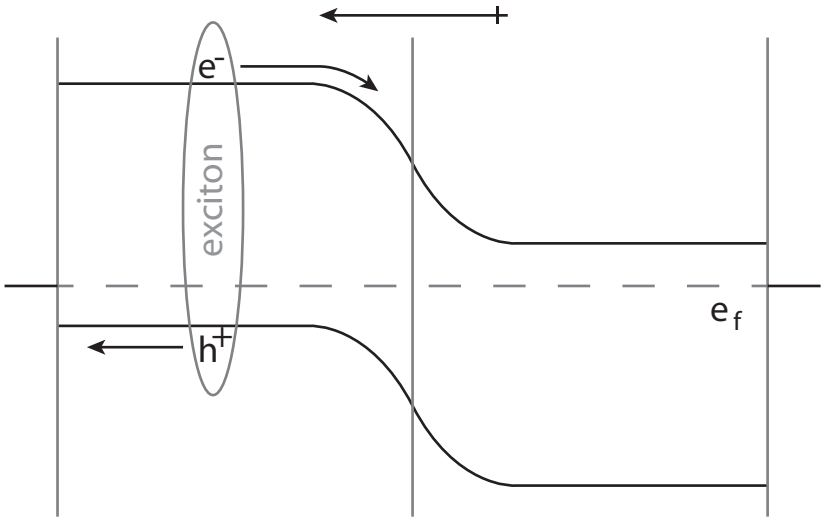

Figure 1.1. A band-bending diagram of a p-n diode, which form the basis of conventional inorganic solar cells. A photogenerated exciton rapidly separates into an a free electron (e^-) and hole (h^+), which can move according to the influence of an interfacial electric field.

In organic photovoltaics (OPV), the process differs from the moment of photon absorption. Organic semiconductors do not possess the high dielectric constant of their inorganic counterparts, and as a result the charge pair of a photogenerated exciton are much more strongly bound. Furthermore, in conjugated organic systems there is much stronger vibronic coupling, which leads to a greater degree of localization[11,12] (to minimize the energy of the geometric distortion). As a result, photogenerated excitons in organic semiconductors tend to stay bound.[13-15] These excitons are expressed as partially delocalized pairs of unbonded orbitals known as geminate soliton or polaron pairs.[16] While they do not spontaneously separate like excitons in inorganic semiconductors, they possess long enough lifetimes to diffuse some distance before collapsing back to the ground state. Unlike

photogenerated free carriers, these charge pairs do not experience electric fields as a motive force. For this reason, and for others to be discussed later, organic photovoltaics are often fabricated as heterojunctions (Figure 1.2). Here there are no long-range interfacial fields, and the exciton must diffuse to the interface at random. There, the energy level offset between the so-called donor and acceptor materials finally provides sufficient motive to separate the exciton into its respective charge carriers.[17,18]

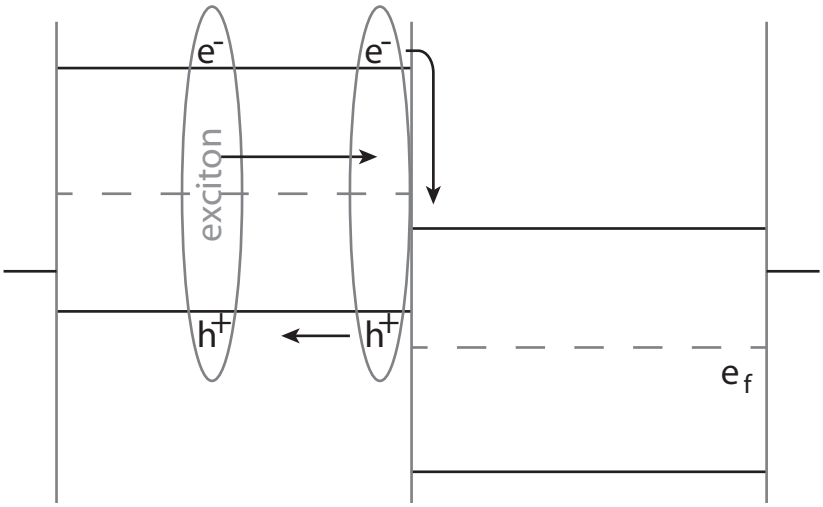

Figure 1.2. An undoped heterojunction, used in place of a p-n junction in OPV devices. In this case the photogenerated exciton remains bound until it diffuses to the donor/acceptor interface, where it can separate into charge carriers.

This process is thought to be mediated by charge transfer (CT) states localized at the interface.[19,20] Carriers thus separated can be transferred to the electron and hole contacts as so-called "charged solitons"[21] (or polarons), so long as they do not recombine at the donor-acceptor interface. While this has proved a more promising approach to organic photovoltaics, planar heterojunctions devices still exhibited

disappointing PCE's. However, the unique fabrication options of soluble organic semiconductors offered a route for improvement: the interfacial surface area could be vastly increased by an intermixing of the donor and acceptor phases. The so-called "bulk heterojunction" utilized a nanoscale separation between the two phases by depositing both from a single solution. Meanwhile the high absorption coefficient offered by conjugated polymers allowed the overall device thickness small enough for both phases to form a contiguous connection two traditional planar electrode contacts. This architecture[22] forms the basis of most modern organic photovoltaics.

Another area where organic semiconductors are used in a manner analogous to, but dissimilar from traditional semiconductors is in the fabrication of light-emitting diodes[23]. These devices, referred to variably as organic light-emitting diodes (OLED's) or polymer light emitting diodes (PLED's) represent the most successful commercial application of organic semiconductors thus far. But as with OPV, successful utilization of these materials has demanded a deviation from the model of conventional inorganic devices. In both organic and inorganic LED's light emission results from recombination of electrons and holes injected on opposite sides of the device somewhere in semiconducting material. In inorganic LEDs the structure, as with solar cells, is fundamentally a P-N junction, in this case operated under forward bias. The differential doping of each side ensures that recombination occurs somewhere in the middle while supporting a high current density.

OLED and PLED devices, by contrast, do not generally rely on differentially doped semiconductors. They may be formed from a single layer of undoped semiconductor, sandwiched between two electrodes matched to the HOMO and LUMO energy levels, respectively. OLEDs may also rely on interfacing two materials, but as with OPV devices, in the form of an undoped heterojunction (Figure 1.3). In either case, for appropriately selected electrode materials, current through the system is generally space-charge limited[23] (the buildup of charge in the semiconductor from injected carriers inhibits the injection of further carriers). This condition limits the current density, and thus luminous flux, of the resulting device, and is not mirrored in inorganic semiconductors where p- and n-doped regions carry a high density of current to the recombination zone. This conspicuous difference leads us to question why OLED and OPV devices do not take advantage of the apparent benefits conferred by p-n junctions.

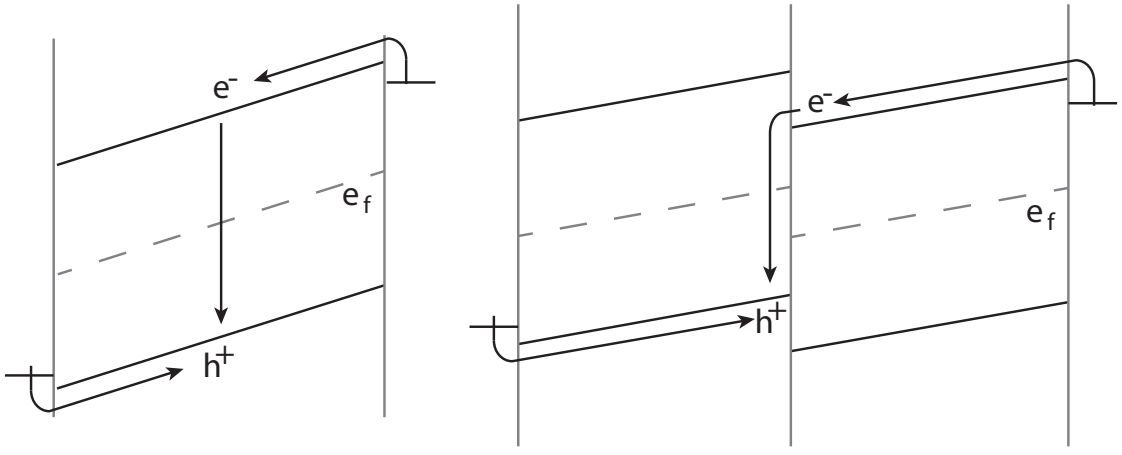

Figure 1.3. OLED device architecture. Electrons and holes are injected from low and high work function electrodes, respectively, recombining in the semiconductor to emit light. Separate e^- and h^+ transport layers may be used, or both functions may be combined in a single layer.

The shift away from the p-n junction in organic semiconducting devices reveals some important differences between the two materials when it comes to doping. The first difference is the significantly higher mobility of ionic species in polymeric or small-molecule matrixes vs. inorganic crystals. The dopants in inorganic semiconductors characteristically inhabit lattice sites, and are fixed at room temperature. Dopant ions introduced to organic semiconductors, on the other hand, occupy the interstitial sites between the polymer chains or small molecules, and even at room temperature can generally respond to electric fields.[24] Dopant diffusion provides a mechanism by which a polymeric p-n junction will, over time, revert to an undoped polymer containing salt[25] (see Figure 1.4).

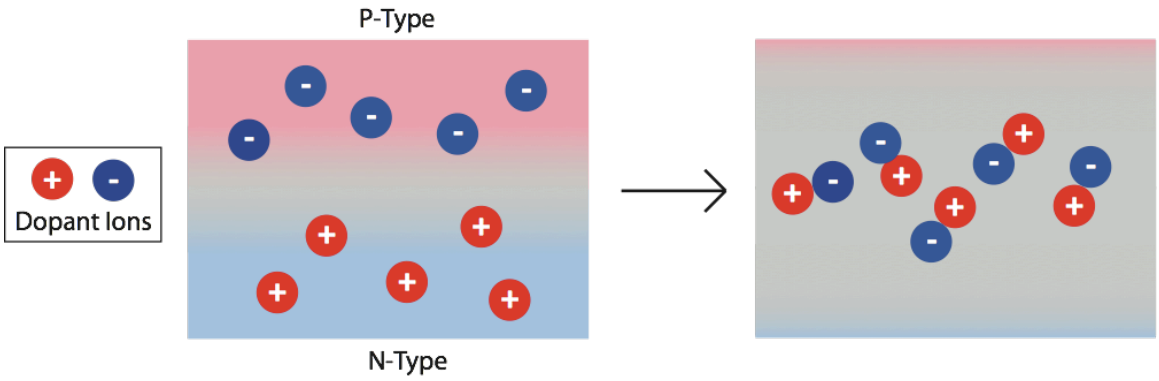

Figure 1.4. An organic p-n junction with mobile dopant ions spontaneously de-doping to form salt and intrinsic material (gray).

It should be noted that there are approaches to stably doping organic semiconductors. One of these is to select a polymeric dopant, which will necessarily have a very low mobility. An example of this strategy is the ubiquitous p-doped

polymer combination poly-(3,4-ethylenedioxythiophene)/polystyrene sulfonate (PEDOT/PSS).[26] This combination enables the formation of p-doped polythiophene without mobile dopants. Similarly, dopants may be immobilized by binding them directly to the conjugated polymer.[25] This method will be discussed in further detail below, for now it should merely be noted that because synthesis of conjugated polymers in their doped form is not feasible, these materials must be fabricated with free counter-ions which must be removed from the material in the course of doping.

Nevertheless, despite the availability of techniques to immobilize dopants, the p-n junction does not feature prominently in the use of organic semiconductors. While PEDOT/PSS and other p-type semiconductors are now widely utilized, they tend to still be used as electrode contacts or interfaced with undoped substrates. This may be largely explained by one of the other distinctions between organic and inorganic semiconductors, namely the significantly lesser stability of the former, particularly in the presence of oxygen. Early conjugated polymers were almost unanimously unstable with prolonged exposure to air.[27] Some air stable systems have been developed,[28,29] but it is still a common issue, prompting considerable research into encapsulation techniques. However the greatest problems with stability have always been associated with n-doped organic systems, which are obviously most susceptible to oxidation. This makes both the fabrication and long-term storage of devices containing n-doped organic semiconductors highly impractical. Thus the heterojunction structure still forms the core of organic semiconductor charge-separation (OPV) or charge-recombination (OLED) devices.

As demonstrated by the above examples, effective use of organic semiconductors in familiar device structures has required a careful consideration of their unique characteristics. In large part, this is to compensate for certain qualities of organic semiconductors, such as decreased stability and stronger exciton binding, which are disadvantageous in these applications. However, the distinctive attributes of organic semiconductors can also provide opportunities, enabling mechanisms of action unavailable to traditional inorganic semiconductors. Qualities that in other contexts would serve as a detriment can be used to novel effect. An excellent example of this useful appropriation relates to the high mobility of dopants in organic semiconductors. While this has previously foiled attempts to create polymer p-n junctions, the broader phenomenon of mobile ions in organic semiconductors has opened up a promising field of new opportunities, accompanied by a growing interest on the part of researchers.

1.3. Mixed Ionic-Electronic Conductor Applications

The field of mixed ionic-electronic conductors (MIEC's) examines the dynamics and application of materials that support both ionic and electronic charge carriers simultaneously. They are often, though not necessarily, composed of organic semiconductors. Those MIEC's that are composed of conjugated polymers also go by the name conjugated polyelectrolytes. The high mobility of ions observed in many conjugated polymers is not a result of intentional design, but polymers such

as polyethylene oxide have a long history of use as ion conductors in applications such as electrolytic capacitors and batteries[30,31]. Both of these applications require the ionic conductor to be electrically insulating, but a semiconducting material that concurrently displays ionic and electronic conductivity offers interesting new possibilities. The collection of MIEC applications presented below will demonstrate the motivation for fundamental research into MIEC's, but it will also provide the context for that research. Organic semiconductor research as a whole is largely an application-driven field, so even fundamental studies, such as those to be described in this dissertation, tend to be conducted with relation to a particular device structure.

One of the more promising approaches to alternative photovoltaics, the dye-sensitized solar cell (DSC), is based around a uniquely complex MIEC system.[32,33] Many MIEC's use a single phase, joint ionic and electronic conductor, but dye-sensitized solar cells are an example of the other approach: separate ionic and electronic conducting phases intimately mixed. The two phases in DSC's are a TiO_2 electron-conducting phase and an electrolyte phase capable of conducting I^- and I_3^- anions. Separating these phases, on the surface of the TiO_2 particles, an organic dye serves as a light absorber. This system involves not only the simultaneous conduction of ionic and electronic charge but also an electrochemical exchange of charge between the phases. Excitons on the dye inject electrons into the TiO_2 phase, and are subsequently reduced by the I^-/I_3^- redox couple, which in turn serves to conduct positive charge. Charge conducted through these phases is collected at opposite electrodes. The DSC system may be thought of as the MIEC variant of the

bulk heterojunction OPV, where the hole conduction phase is now electrochemical. The DSC system is worth mentioning as one of the most promising recent MIEC systems, but it should be noted that the intentional use of electrochemical exchange between ionic and electronic systems is the exception, rather than the rule in MIEC's. In most MIEC systems, electrochemical oxidation/reduction of the ions would constitute a degradation pathway, and where possible ions are often selected to be electrochemically stable.

As the dye-sensitized solar cell is the MIEC analog of the bulk heterojunction OPV, the polymer light-emitting electrochemical cell (PLEC) shares the same relationship with the OLED/PLED device. A PLEC would in many cases be identical in construction to a conventional PLED device, except that the active material(s) contain a significant concentration of mobile ions[34]. While the materials of a PLEC contain ions, they are generally intrinsically undoped (the net ionic charge is 0). One or both of the ions may be mobile, and the MIEC may comprise one or two phases.[35] In spite of the name, the ionic constituents of polymer light-emitting electrochemical cells are generally electrochemically stable at operating voltages. This means that so long as the electrode interfaces are ion blocking (which they invariably are) there is no net ionic current at equilibrium. PLEC's have been found to have a much slower response than PLED's, although they also display a significantly reduced operating voltage.[36] If the structural differences of the PLEC system are comparatively simple, the mechanism of operation is certainly not. PLEC research has been the source of an expansive and sometimes contentious dialogue

about the fundamental physics of MIEC devices, which will be explored in greater detail below.

MIEC's have also found their way into transistors, in the form of electrolyte-gated transistors.[37,38] The term "electrolyte gated transistor" can refer to several different device structures. In one case, it merely means a transistor whose gate is composed of an electrolytic capacitor, but where the semiconducting material, organic or inorganic, is ion blocking. In this case the functional mechanism is identical to a normal field-effect transistor, and these are not properly considered MIEC systems. However, when the channel of the transistor is a thin film of organic semiconductor (devices known as OTFT's), then potential between the gate and channel may drive ions into the latter, doping it. In this case, the channel of the transistor is essentially an MIEC with a variable doping level. While ion mobility limits the switching speed, these structures provide the potential for lower voltage response.[37] Additionally, the sensitivity of electrolyte gated transistors to ions has enabled the appropriation of these systems for biosensors.[39] As with conventional field-effect transistors[40], electrolyte-gated transistors are useful not only in functional devices but in the fabrication of model systems to study the effects of doping concentration.

The adjustable doping afforded by MIEC structures also enables electrochromic devices, which are not light-emitting but change color depending on applied voltage.[41] This is possible because of the tendency of conjugated polymers to carry injected charge in newly generated electronic states called solitons[11] or

polarons (depending on the symmetry of the polymer). These states correspond to partially delocalized unbonded orbitals, either filled (- charge) or empty (+ charge). They necessarily lie in the band gap, so the transitions associated with these states will be redshifted from the band gap absorption of the polymer,[42,43] appearing somewhere in the visible-NIR. Sufficiently high levels of doping can lead to bleaching of the band gap absorption as well.

Finally, MIEC's have recently found increasing use in charge injection layers[44]. As organic semiconducting devices have grown more refined, researchers working on a number of different applications have come to recognize the importance of charge injection layers, usually between the electrode contacts and the active materials of a device. Charge injection layers serve two purposes. First, they serve as selective contacts, designated as either electron or hole injecting layers. The work function of metal electrode contacts is of course selected with a similar goal in mind, but the metals themselves are adept at delivering either sign of carrier, and have often been found to serve as efficient recombination centers.[45] Electrode surface recombination is especially crippling in applications such as bulk heterojunction OPV's where donor and acceptor material are both in extensive contact with each other's electrodes.[46] Thin layers of appropriately selected semiconducting materials, particularly if they preferentially pass one sign of carrier,[47] can be used to reduce the surface concentration of undesired charge carriers.

The second purpose served by charge injection layers is to lower barriers to charge injection. Mismatch between the semiconductor valence or conduction band and the electrode work function can introduce barriers to charge injection (or extraction). This is a special concern at the cathode, where metals with an appropriately low work function (such as Ca or Ba) tend to be reactive and/or electrochemically unstable. There are various approaches to achieving this barrier lowering, but the strategy of inserting thin MIEC layers has met with considerable success.[48,49] While the phenomenon is still the subject of ongoing research, it seems that there is a common mechanism behind the lowering of operating voltages observed in PLEC's, electrolyte-gated transistors, and MIEC injection layers. This mechanism will be discussed further below.

1.4. MIEC Device Physics

The collection of MIEC applications presented above spans a broad range of different device architectures and materials. However, these device structures share some common behavioral characteristics. The most obvious of these are an increase in response time, and a decrease in operating voltage. Both of these characteristics are now understood to result from ion motion in response to applied potential.

As will be seen, the profile of ions throughout an MIEC system can have a profound effect on the electronic characteristics, but since the ionic mobility is much lower than the electronic, the approach to equilibrium is much slower in an MIEC than in a purely electronic conductor. The response time of MIEC systems to applied bias varies from a fraction of a second to hours, depending on the material and the particular structure.

The decrease in operating voltage is largely understood to result from the accumulation of ions at the interfaces of the MIEC material.[50] The establishment of a double layer at the interface compresses barriers to injection by enabling a strong electric field in the MIEC adjacent to the interface (see Figure 1.5).

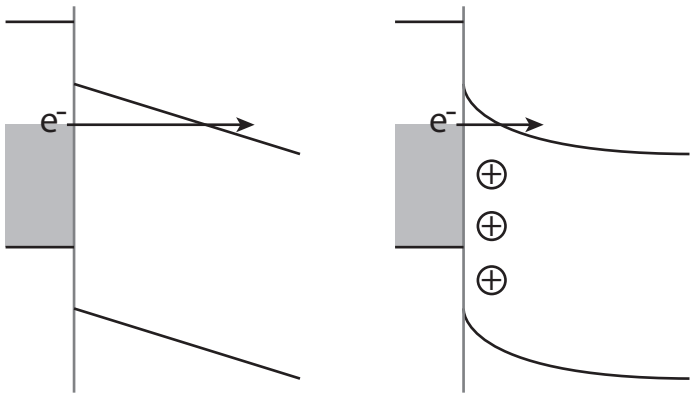

Figure 1.5. Enhancement of electron injection at the electrode interface with an MIEC (right) vs. an undoped semiconductor (left). In the latter case, bias is dropped uniformly across the width of the semiconductor (neglecting space-charge effects) while in the former case accumulation of ions compresses the potential drop against the electrode interface. This decreases the length of tunneling required to reach the conduction band.

Beyond the effect of ions at the MIEC surface, however, there is less unanimity as to what occurs in the bulk of the material. Charge transport through MIEC's has been treated differently depending on which device structure they are incorporated into, and even within a given field there are often competing models.

Some of the earliest studies into MIEC charge transport were conducted under the label of "redox conduction", in mixed-valent polymers.[51,52] The materials were generally coordination polymers containing metal ions serving as discrete redox sites, where carrier conduction occurs via hopping transport between sites. While this picture differs slightly from the model of semi-delocalized mobile carriers employed for most conjugated polymers, hopping transport is commonly used to describe both materials.[53,54] Mixed-valent polymers constitute MIEC's because the positively charged redox sites are accompanied by counter ions. Additionally, the material in these studies was often saturated with electrolyte. The model of redox conduction is comparatively simple but informative, and particularly insightful about the nature of the polymer-electrode interface. Any applied potential is assumed to be screened by the high concentration of ions. Transport of carriers through the system is diffusive, in this case a linear gradient of reduced to oxidized sites is envisaged across the film.[51] Injection of carriers at the electrode is viewed as an electrochemical process, where the concentration is determined by the potential drop between that electrode and the bulk, and by the Nernst equation. Experimentally, it is important to note that the mixed-valence polymer in this system formed the working electrode of a three-electrode electrochemical cell, so

the quantity of ions in the polymer was not fixed, and total charge neutrality could be insured regardless of the level of injection.

While this early research was not performed with reference to any particular application, the experimental setup makes for a natural comparison to the electrolyte-gated transistor research that was to follow.[38] While electrolyte-gated transistors do not generally feature a reference, the gate-electrolyte interface enables a significant quantity of charge to be moved out of the MIEC system entirely, allowing the carrier distribution to be determined by the Nernst potential and Fick's laws of diffusion.

The model describing dye-sensitized solar cells shares some similarities with the model described above.[55] The electrolytes which saturate DSC's are understood to screen electric fields, and conduction of both electronic and ionic carriers is diffusive, although in this case the carrier flux and concentration profiles are altered by the continuous generation of carriers throughout the film.

These models provide valuable insights for understanding MIEC behavior, but they also contain simplifying elements, such as a saturating electrolyte and the presence of an external counter electrode, which do not correspond to most device structures. The most relevant and comprehensive field of study into the dynamics of MIEC systems comes from PLEC-related research. Polymer light-emitting electrochemical cells are of a distinctly *less* electrochemical nature than the systems modeled above. The systems do not (intentionally) contain any solvent, so only the residual ion conductivity of the polymer enables equilibration of ions. The term

"Equilibration" is appropriate because ions are picked to be electrochemically stable, so they do not participate in ongoing charge transport. This is not to say that they do not affect the ongoing electronic transport, because the distribution of ions is extremely important, both at the MIEC interfaces and in the bulk.

Traditionally, two competing models have been applied to understand bulk conduction in PLEC's. The electrodynamic model[56] (ED) describes a picture somewhat similar to the models described above. The field is screened, which is to say that the applied bias is dropped in double layers at the electrode interfaces. These double layers lead to enhanced carrier injection at both electrodes (although this injection process is not necessarily considered to be Nernstian), though the screened field limits conduction to diffusion. The carrier profiles demanded by diffusive transport may be compensated by a similar profile of ions (see Figure 1.6). At some point in the profile, injected electron and holes meet and recombine. The simplest forms of this model assume both signs of ion to be mobile, although the dynamics do not substantially change if one of them is fixed.

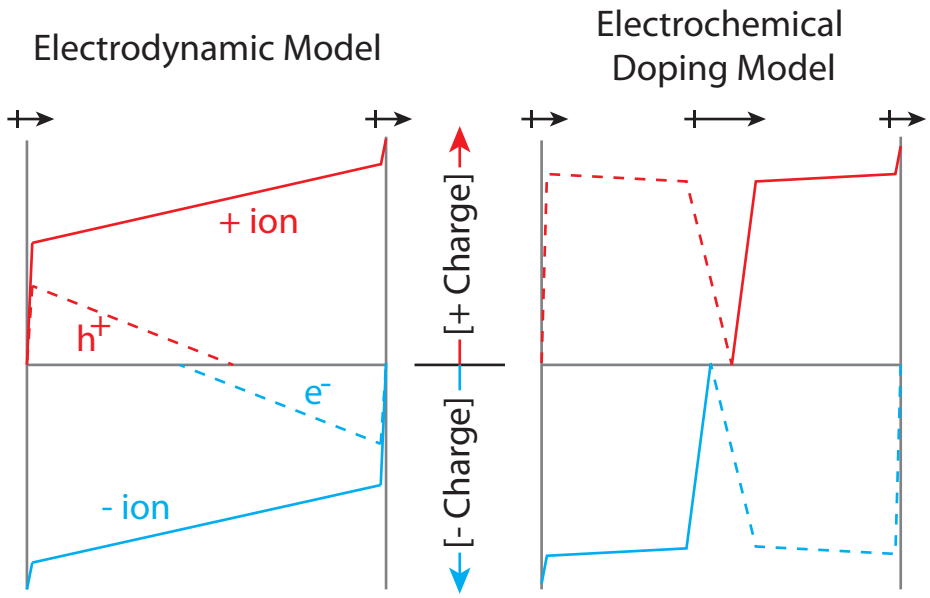

Figure 1.6. Concentration of ions (—) and electronic charge carriers (---) across the width of PLEC devices operating under the electrodynamic and electrochemical doping model. Concentration of positive carriers is registered above the *x* axis and negative carriers below. The location of significant potential drops is indicated as electric fields above the diagrams.

The so-called electrochemical doping model[34,36] (ECD), on the other hand, emerges from an understanding of MIEC's formed by studying doped polymers. Doping of polymers is often achieved electrochemically, biasing the material in a three-electrode configuration such that ions are either drawn in or expelled with the injection of electronic charge. In the ECD conception of PLEC's, the interfacial dipoles drop just enough of the applied potential to form ohmic contacts, and then two doping fronts sweep inward, segregating the ions as they progress and forming conductive channels which facilitate further doping. Conduction in these channels is driven by a combination of drift and diffusion.[57] Somewhere in the middle the p-doped and n-doped regions meet, and a depletion region analogous to that of a

conventional p-n diode forms. Across this region recombination occurs and the majority of the applied bias is dropped.

When comparing these models, it should be noted that the distinction between a doped polymer and an undoped one with locally compensated injected carriers, is unclear. However the models do make substantially different predictions in some respects, especially with regards to the electrostatic potential drops across the system. This dispute has been largely supported by the difficulty of directly measuring what happens in experimental devices beyond the interfacial dipoles. However, an illuminating series of experiments with open-face devices has finally provided conclusive evidence, in support of both models.[58] In other words it was shown, to the vindication of some theorists,[59] that the ED and ECD models are limiting cases of a common system. The ED model will predominate except when the levels of injected charge rise high enough to match the mobile ion density, at which point the ECD model will start to be more appropriate.

As previously mentioned, PLEC structures do not have an external counter electrode that can be relied upon to ensure total charge neutrality. However, consistent with the desired mode of operation, both models of PLEC conduction assume bipolar injection, so the issue of total charge neutrality is not explicitly addressed. In the case of appropriately constructed PLEC devices, this assumption is probably accurate, but this is an important point to consider when trying to apply these models to more general systems.

1.5. Experimental Evidence in MIEC Models

The variety of different models available to describe MEIC charge transport does not necessarily represent controversy or uncertainty. Different models are appropriate for different systems, and as ED/ECD shows, sometimes for even the same system operating in different regimes. However, even for well established devices, controversies and misunderstandings over the basic qualitative picture persist. Meanwhile, quantitative measurements of various material parameters, such as carrier mobility, doping level, and recombination rate constant, are often unattainable. Both problems are representative of the difficulty of interpreting traditional electronic measurements in MIEC systems. Steady-state electronic measurements[60,61] are hard to quantitatively interpret when they incorporate the influence of an unknown profile of ions. Time-variant electronic measurements,[62,63] which might otherwise resolve some of these issues, are unclear when the response of electronic carriers is convoluted with the ionic response. Neither system may be comprehensively modeled without accounting for the behavior of the other, and the material parameters which might conceivably be used to construct a holistic model are often unavailable because of the aforementioned convolution.

The need for additional lines of evidence is clear. This was shown to great effect when scanning Kelvin probe microscopy on open-face PLEC devices was used to determine the potential-drop profile,[58] measurements which went a long way to clearing the ED/ECD controversy. However this is not a magic bullet, many device

structures cannot be fabricated in open-face geometry. Additionally, since open-face devices are effectively much thicker than their conventional sandwich-structure counterparts, they may not accurately represent mechanisms which involve capacitive effects at the electrode interfaces. Techniques to probe the internal dynamics of MIEC systems in more conventional architecture are needed.

The field of organic semiconductors as a whole shows how, with time, a fundamental understanding of new and radically different materials can lead to their successful application. The novel behavior of organic MIEC systems offer the potential for improving existing device structures, as well as uncovering entirely unforeseen applications. However, this will require the considerable barriers to MIEC characterization to be overcome.

1.6. Dissertation Overview

This dissertation is organized in three chapters, exploring both quantitative and qualitative characterization of MIEC systems. All chapters are linked by the common theme of combining NIR absorbance measurements of carrier density with more conventional electrical measurements to gain insight into the internal dynamics of MIEC's. Chapter II will give an introduction to the technique, and its use in determining material parameters, while Chapters III and IV will examine the dynamics of more complex and application-relevant device architectures.

1.6.1. Chapter II

This chapter will discuss determination of a concentration-dependant carrier mobility in an MIEC system by simultaneous measurement of current and injected carrier density using NIR absorbance. The primary purpose of this chapter is not to report the value of mobility, but rather to demonstrate a technique by which this and other parameters may be determined in MIEC materials which often confound conventional measurement techniques. A general model of charge transport in this and similar systems will be also discussed. Finally, the technique of NIR absorbance will be used to evaluate the efficacy of another approach to gathering injected carrier density; short-circuit discharge measurements. This chapter was previously published in the Journal of Physic Chemistry C, coauthored with Mark C. Lonergan.

1.6.2. Chapter III

The third chapter concerns the construction of a more detailed model of charge transport in MIEC systems in the unipolar injection regime, as would be expected for a charge injection layer. Specifically, the interactions between the MIEC and the contacting electrodes will be considered, exploring a phenomenon of rectification when one of the contacts is a semiconductor. A model describing this

process and the situations where it is relevant will be presented, and then experimentally demonstrated using an MIEC with gold and p-type Si contacts. This chapter contains material that is to be submitted for publication in the Journal of Physical Chemistry Letters, coauthored with Mark C. Lonergan.

1.6.3. Chapter IV

This chapter will investigate the junction formed between MIEC materials with differential ion mobilities. Specifically, the interface will be studied between two functionalized polyacetylenes, each possessing a fixed ion and mobile counter ion, with an inversion of sign between the materials. This "hetero-ionic junction" constitutes an ionic p-n junction, and the role of ionic asymmetry in the electronic behavior of this system will be investigated, particularly as it pertains to the photovoltaic behavior. This chapter was rewritten and reformatted from an article published in the Journal of Physical Chemistry Letters, coauthored with Fuding Lin and Mark C. Lonergan.

CHAPTER II

CHARACTERIZING CHARGE INJECTION, TRANSPORT, AND MOBILITY IN A CONJUGATED POLYELECTROLYTE BY NIR ABSORBANCE

Reproduced from Walker, E. M. & Lonergan, M. C.. *J. Phys. Chem. C* 14929–14938 (2013). I performed the experiments and analysis, with helpful discussion and editorial oversight by Mark Lonergan.

2.1. Introduction

Organic semiconductors containing mobile ions, in particular conjugated polyelectrolytes, have been the subject of significant interest in recent years,[64,65] yet characterization of charge transport in these materials has proven difficult. Charge transport in bulk semiconducting materials is generally characterized in terms of the carrier mobility μ; however, traditional methods of measuring mobility are complicated by the presence of a significant concentration of mobile ions. For measuring carrier mobility in organic semiconductors, the current response of a sandwich device to pulsed,[62] or linearly increasing[63] voltages is often utilized.

However, in the case of materials containing mobile ionic components, the response due to the electronic carriers is often convoluted with the response of the ions to that same changing field. On the other hand, measurement techniques that rely on a static applied voltage such as time-of-flight (TOF)[66,67] or space-charge-limited current (SCLC)[60,61] are compromised by the partial or complete screening of the internal electric field by those same mobile ions. With sufficiently low ion mobilities, the space-charge limited current model may be applied to I-V measurements performed as a series of millisecond-scale pulses.[68,69,70,71] However, this technique is clearly not suitable for probing the mobility under DC conditions where ion polarization enables higher injected carrier densities. Capacitance-conductance (CC) measurements in organic field-effect transistors (OFET's) have also been a valuable tool in determining mobility.[1,72,73] Unfortunately, the control of carrier density through gate voltage that enables these measurement is similarly impeded by the field-induced accumulation of mobile ions on the insulator interface.

Another impediment to determining mobility for conjugated polyelectrolytes is reliable modeling of the mechanism of conduction. Mobility measurements are almost always dependent on some model of the field and charge profile within the device. Current response to pulsed or linearly increasing voltage, as well as TOF measurements rely on models of carrier behavior to translate the current transients into mobility.[8,62,63,66,67] Meanwhile steady-state measurements techniques such as SCLC and CC in FET's rely on a model to determine the quantity of injected charge,[13,61,72] a necessity for translating current into mobility. Assigning the most accurate model of conduction can be an uncertain enterprise in many systems, but it

is particularly perilous when an additional set of mobile charge carriers (namely ions) is not accounted for. Another challenge for appropriate modeling comes from the possibility of concentration or field-dependent mobilities. Such dependencies further complicate the task of assigning an accurate conduction model, making it difficult to ascertain whether unexpected current behavior is due to a non-constant mobility or dynamics unaccounted for by the model, such as intrinsic carriers or bipolar injection. Field-dependent mobilities have been extracted from SCLC measurements,[19,71] but the ambiguity between field and concentration dependence in this measurement requires that the approach be validated by models of the expected field dependence.

A potential method for addressing uncertainty about conduction mechanism, as well as the interfering qualities of mobile ions, is to directly measure the quantity of injected charge. The relation between injected charge and voltage can be very useful in confirming whether the assigned model is appropriate. Additionally, current-voltage behavior alone can be a poor indicator of the actual injected charge, particularly when mobile ions are present. In these systems, direct measurement may offer the only approach to determining mobility. Finally, the addition of a third measured parameter (in addition to current and voltage) would allow us to more confidently approach systems where the mobility is likely dependent on field or on concentration.[23,74] In particular, if the electric field inside the material is well quantified, the relation between charge and current can be especially valuable in extracting concentration-dependent mobilities. One method of measuring injected charge previously used in conjugated polyelectrolyte systems is the integration of

the current released when a previously biased sample is discharged under short-circuit conditions.[23,34,75] In the specific case of dye-sensitized solar cells, selective electrodes combine with an extraordinarily low recombination rate to enable near-total collection of charge.[32,33,76] However, in most other systems internal recombination cannot be so easily discounted, and so accuracy of this technique is reliant on its own model of how much of the injected charge recombines internally instead of across the short-circuited leads.

Our goal in this study is to utilize near-infrared absorbance spectroscopy to characterize the charge-voltage relationship in a conjugated polyelectrolyte conductor. While ionic motion in this material precludes measurement of mobility by the more conventional means outlined above, it also leads to a high density of injected charge in a mechanism analogous to electrochemical doping. We aim to show that in conjunction with the measured current-voltage relationships, quantification of injected charge by NIR absorbance may be used to illuminate the mechanism of charge injection and transport in a system with mobile ions. Additionally, we may ascertain the carrier mobility, even when it displays a strong dependence on concentration. In the course of these studies we also collect post-bias short-circuit measurements, to better characterize the discharge behavior and ascertain the validity of this method. Our approach is enabled by the carrier-induced NIR absorbance of our conjugated polyelectrolyte, and we approach mobility through the diffusion coefficient, which may be determined based on the charge-current relationship.

The material used in this study is a cationically functionalized polyacetylene (Figure 2.1). This material exhibits an interesting electrical dynamic where the local concentration of positive ions is fixed throughout the material, but the negative counter-ions are free to move in response to bias. Such materials display utility as mixed-ionic electronic conductors as well as in the preparation of organic P-N junctions.[25,37,38,77] As with many conjugated polymers, polyacetylene displays a NIR absorption band in response to injected charge.[39,78,79] Polaron or soliton induced absorptions have been shown to be useful for the characterization of charge carriers in a number of systems. [41,80,51,52,81,51,82] In polyacetylene specifically, both the IR[55,83] and NIR[59,84,64,65,85] absorbance bands have been utilized. For our measurements, the NIR band was employed, and quantification was enabled by first measuring the carrier extinction coefficient using electrochemical doping.

Following quantification by absorbance (Figure 2.2), the charge injection density was used to calculate the mobility. In addition to carrier concentration, determination of mobility from a steady-state measurement also generally requires knowledge of the internal electric field. This would seem difficult due to the presence of mobile ions. However, with even moderate ion densities, it is expected that for low voltages the field will be screened completely and current will be diffusion-limited.[56,62,59,63] This screening of the electric field means that in the presence of mobile ions, the carrier mobility is best obtained by measuring the carrier diffusion coefficient D and then using the Einstein relation $D=\mu k_B T/q$. In previous studies,[51,66,86] charge transport by diffusion has been measured in electrochemically doped redox polymers. As in this approach, our calculations rely

on the steady-state current and a carrier concentration profile, which was inferred from a measured carrier density. What distinguishes our approach is its application to an initially intrinsic system where charge injection is a product of response to applied bias.

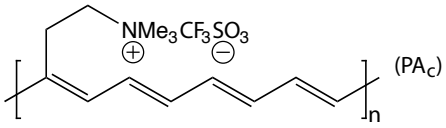

Figure 2.1. Cationically functionalized polyacetylene with mobile triflate anions, hereafter referred to as PA_C.

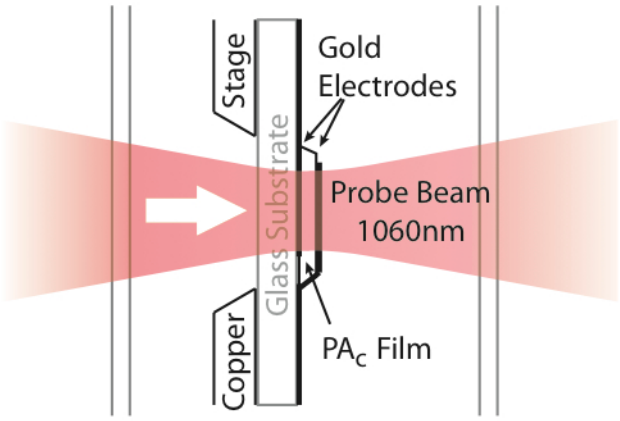

Figure 2.2. Experimental geometry: a PA_C thin film sandwiched between two semi-transparent gold electrodes. The sample is held under vacuum and heated to 45° C, while the NIR probe beam is focused within the sample area.

2.2. Experimental

PA_C (see Figure 2.1) was synthesized by a ring-opening metathesis polymerization of the cationically functionalized cyclooctatraene.[67,87] Thin-films were fabricated by spin-coating in air out of a 10mg/ml solution of polymer in DMF onto a 15 nm evaporated gold electrode on a chromium adhesion layer. Oxygen exposure was restricted to several minutes before the evaporation of a 15 nm top gold contact. Together these electrodes attenuated transmitted light by about one absorbance unit. The sample was annealed under vacuum at 125° C for 8 hours to expel bound oxygen and DMF. This step differentiates these experiments from our previously reported measurements on the same material.[60,75] I-V and absorbance measurements were then performed under vacuum on a temperature-controlled chuck (see Figure 2.2), where the sample was held at 45° C to enhance ion conductivity. A series of applied voltages, each four hours long, were separated by eight hours of relaxation under short circuit (0 V applied bias). The current during the short circuit was also recorded. Using a monochrometer with a tungsten halogen light source, a probe beam was focused within the 4 mm sample area, and subsequently measured using an InGaAs detector in short-circuit mode. The measured transmittance was corrected for the simultaneously measured light source intensity. After the completion of measurements, the film thickness (~480 nm) was determined by cutting a series of lines through the structure and examining with an optical profilometer.

Measurement of the absorbance coefficient of injected charge was performed in an airfree three-electrode spectro-electrochemical cell using samples between gold electrodes prepared in the manner described above. A 0.075 M tetramethylammonium tetrafluoroborate solution in acetonitrile was used as the electrolyte with a Pt counter electrode and a Ag-$AgNO_3$ reference at 0.283 V vs SCE. The top and bottom porous gold electrodes on the samples were connected together to function as the working electrode. While doping, the visible and NIR absorbance through the films was measured using diode-array spectrometers. To verify that the absorbance coefficient in the dry polymer was the same as when swollen with solvent, a sample was trapped in a doped state by removing the electrolyte in the midst of doping. Airfree conditions were then maintained while washing with acetonitrile. Absorbance measurements were continued while the sample was dried under vacuum.

Dry ammonia for compensating p-type carriers was obtained by equilibrating an evacuated airfree vessel containing $CaSO_4$ with the head space of a vessel of degassed 30% aqueous ammonia at room temperature. This vessel was subsequently opened to the sample vacuum chamber (of lesser volume) by an evacuated line. After being biased at 1.5 V for 10 minutes, the sample was exposed to ammonia for 2 minutes while current and absorbance were measured.

2.3. Results and Discussion

2.3.1. Characterizing Charge Injection and Transport

The primary experiment entailed a series of 4hr static biases to a thin film of PA_C (Figure 2.1) while current density (J) and NIR absorbance were measured. Figures 2.3a and b display the current and the absorbance change for a range of applied biases from 0.5 V to 1.4 V, in 0.1 V steps. Lower voltages did not result in sufficient charge injection to quantify by absorbance. The final point in each trace in Figures 2.3a and b was used as the steady-state current or absorbance. (Figures 2.4a and b).

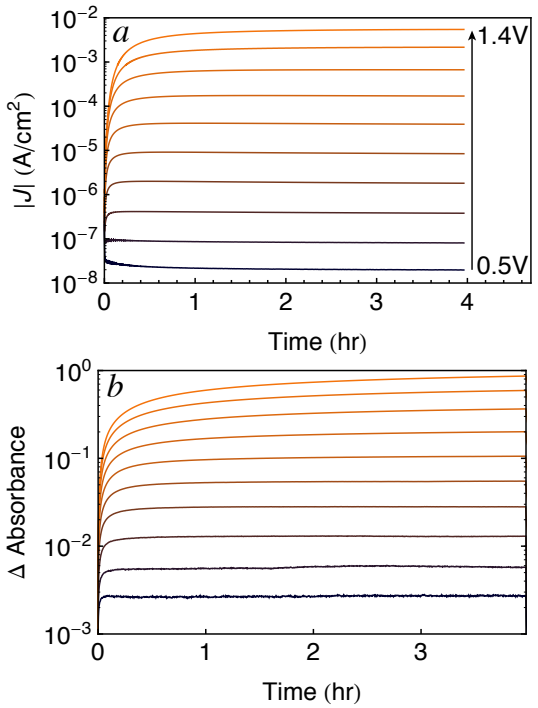

Figure 2.3. Current density (a) and absorbance change at 1060 nm (b) in response to potential steps varying from 0.5 to 1.4 V.

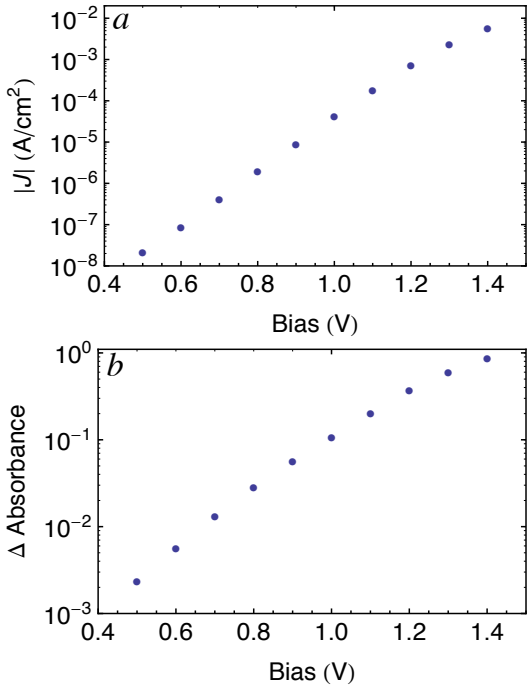

Figure 2.4. Steady-state current density (a) and absorbance change (b), taken from the final points of Figures 2.3a and b as a function of bias.

The absorbance change relative to the fully discharged state (ΔA) may be related to the areal density of injected holes d_h (cm^{-2}) by

$$qd_h = \frac{\Delta A}{\varepsilon} \quad (1)$$

where q is the elementary charge and ε an extinction coefficient. The quantity qd_h is an injected charge density (C/cm^2) describing the total amount of charge injected into a slab of the polymer per unit area. The identification of the charge carriers as holes is discussed further below.

The extinction coefficient ε was experimentally determined on separate calibration samples by measuring the absorbance change while electrochemically p-

doping. Samples were doped in a three-electrode electrochemical cell, with a film of the polymer sandwiched between two gold electrodes used as the working electrode. The sandwich geometry was used to closely mimic the two-electrode geometry used in electrical characterization. For the electrochemical experiments, the electrode in contact with the electrolyte was sufficiently thin so as to remain porous, which is required for electrochemical doping. The NIR absorbance was measured by a diode-array spectrometer while the sample was p-doped by a cyclic voltammetry sweep (Figure 2.5).

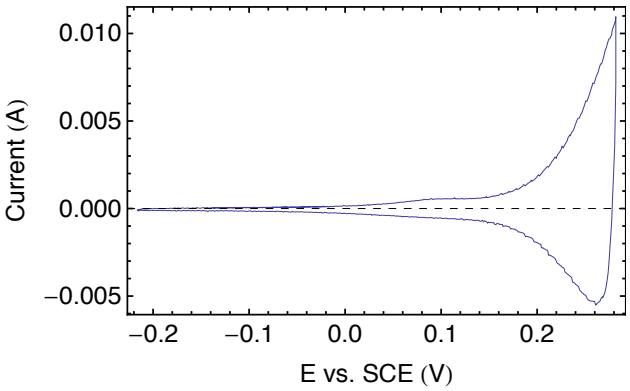

Figure 2.5. p-Doping of a PA_C layer by cyclic voltammetry.

The electrochemical doping of the calibration samples demonstrated the broad NIR absorbance characteristic of charge injection in polyacetylene.[61,79] The acetonitrile electrolyte also exhibits several absorbances in the NIR, but there is a clear window in the region of 1060 nm. Extracting the absorbance change at 1060 nm, and comparing this value to the integrated current density from cyclic voltammetry revealed a clearly linear charge-absorbance relationship (Figure 2.6).

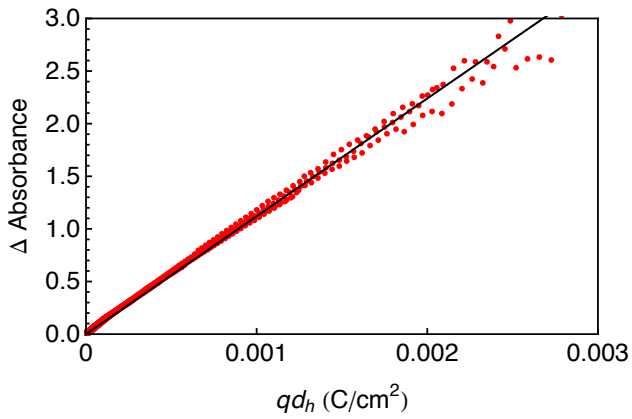

Figure 2.6. Absorbance change at 1060 nm during cyclic voltammetry vs. the corresponding charge injection. Two different samples are overlaid.

The slope of this plot is equal to the extinction coefficient ε. Here ε is found to have a value of 1160 cm^2/C. To verify that this value did not change significantly in dry films relative to the acetonitrile swollen films used for calibration, the absorbance of a doped film was measured after the electrolyte was removed, and the film rinsed with acetonitrile under airfree conditions and dried under vacuum. No significant change was observed.

Applying the obtained value of ε to absorbance measurements made during the applied bias series, the injected density of charge d_h was then determined. The solid circles in Figure 2.7 show the dependence of qd_h on applied bias. At this point in the discussion, we will focus on the experimentally observed charge density. Later we will return to discuss the red and black lines, which display the levels of charge injection expected from different models of charge injection and transport.

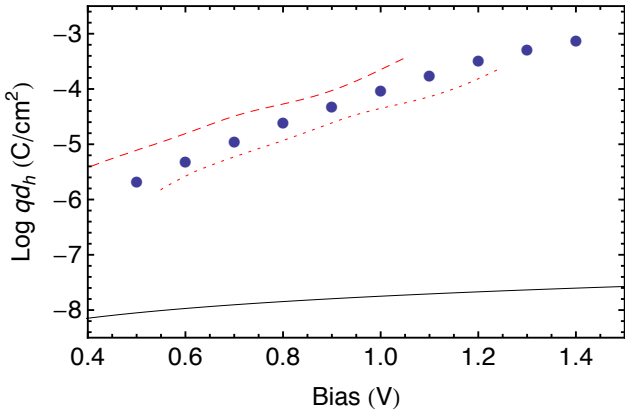

Figure 2.7. Injected charge density across the range of applied bias (•). The solid black line indicates the maximum charge injection expected from a space-charge-limited model (see equation 2), while the dashed red lines are based on a model of electrochemically-supported charge injection (see equations 3 and 4). These models incorporate the integrated current from the cyclic voltammogram shown in Figure 2.5, adjusted using values of 5.05 V (---) and 4.93 V (- - -) vs. vacuum for the Fermi level in the pristine material.

First, the strong dependence of charge on applied bias conclusively demonstrates that the current is not dominated by defects or impurities present in the pristine material. More significantly, the level of charge injection observed greatly exceeds that which would be expected from the space-charge-limited model, where the charge is limited to twice that stored at that voltage in an equivalent parallel plate capacitor:[68,88]

$$qd_h^{SCL} < \frac{2V_{app}k}{l} \qquad (2)$$

Instead of being due to extrinsic impurities (which would not depend on applied bias), this mismatch may be best understood by considering the role of ions

in charge injection. Rather than being space-charge-limited, this material can support additional injection by compensating charges through the shifting of mobile ions. This behavior is supported by the high concentration of ions (on the order of 1×10^{21} cm^{-3}), which significantly exceeds the highest observed concentration of electronic charges. Additionally, the timescale of charge injection, taking hours to reach equilibration (see Figure 2.3) implicates ionic motion as the limiting factor in injection[24,69]. That ion motion is the limiting factor and not, for instance, the activation energy of deep traps, can be inferred from the observation that response time is vastly decreased on exposure to acetonitrile vapor. The acetonitrile swells the polymer and as such would be expected to increase ionic mobility, while having a negative effect, if any, on the electronic conductivity. Therefore, charge injection in this system is more analogous to electrochemical doping, where the injected charges are compensated by electrolyte ions, and any applied bias drops over narrow ionic double layers at the interfaces. More precisely, the concentration of carriers adjacent to the injecting electrode is in quasi-equilibrium with the electrode and would be determined by the portion of the applied bias dropped across that interface, as well as the initial position of the Fermi level in the system.

While the previously described model is hereafter referred to as electrochemically supported charge injection, it is not to be confused with the "electrochemical doping model" often used to describe injection and transport in light-emitting electrochemical cells (LEC's).[58,70,71] While the electrochemical doping model also invokes electrochemically supported charge injection, it implies a different distribution of doping and applied bias. In the electrochemical doping

model, bipolar injection results in a p-i-n junction, with the majority of the bias dropped in the middle of the device. In contrast, our results indicate that charge injection and transport in the low-bias limit of this system is better described by the "electrodynamic model", also commonly applied to LEC's.[56,89] In this model, while the injected carriers in the bulk are still compensated by displaced ions, most of the bias is dropped by ionic double layers at the electrode interfaces, and charge transport in the bulk takes place through diffusion. Evidence supporting both of these models in LEC's has been presented,[58,90,91] including direct measurements of the potential profile through scanning Kelvin probe and electric force microscopy. These results suggest that the distinguishing factors are the rate of carrier injection and the presence of barriers to this injection. Both models often invoke bipolar injection (a necessity for efficient LEC's) though it is not a requirement if one sign of charge carrier is more easily injected than the other. In particular Ginger et al.[90] present evidence for a "preferential p-type model" involving unipolar hole injection. The matter of charge neutrality in the case of unipolar injection is resolved as follows: local charge neutrality is ensured across the film by excess anions matching the injected hole profile. This leaves a depletion region of immobile cations, which are in turn compensated by a buildup of negative charge on the cathode. The same sort of charge balance forms the basis for asymmetric capacitors[92], which combine faradaic and non-faradaic charging on opposite electrodes.

To test the validity of this model of electrochemical injection, the observed charge was compared to the integrated current from the cyclic voltammogram shown in Figure 2.5. Specifically, the red lines shown in Figure 2.7 are calculated by

$$qd_h^{EC} = \eta Q_{CV}(E) \quad (3)$$

where $Q_{CV}(E)$ is the measured charge injection from the CV shown in Figure 2.4, and η is a geometric factor, compensating for the relative thickness of the two different samples, as well as the non-uniform carrier distribution across the two-electrode film (see supporting information). The electrode potential E is related to the applied bias in the two electrode case by:

$$E = \frac{V_{app}}{2} - \mu_0 \quad (4)$$

Here the division of the applied bias between the potential drops at the two electrode interfaces is assumed, for approximation, to be equal. The voltammogram was also adjusted to compensate for the initial Fermi level of the system (μ_0). Because the initial Fermi level is not known precisely, the comparison shows the results for a range of possible values for μ_0 between 4.93 V and 5.05 V vs. vacuum. The former is an estimate of the intrinsic level of the polymer from cyclic voltammetry[93] and the latter adjusts this level for some initial p-type character to the system (see below). That the observed qd_h in the two-electrode system is consistent with electrochemically supported charge injection, and notably dissimilar to the behavior of a space-charge-limited system, lends support to our model of charge injection and transport. Furthermore, with qd_h consistent with the expected value based on quasi-equilibrium with the injecting electrode, we have evidence

that the charge transport is bulk and not interfacially limited. Otherwise the qd_h would be lower, as charges were carried away faster than they could be injected.

One important question remaining is the identity of the injected carriers. The analysis above presumes unipolar injection, both with respect to the space-charge limit (bipolar injection can support higher charge density[94]) and with respect to the estimate based on cyclic voltammetry. Additionally it is important to confirm the identity of the carriers, as the extinction coefficient was determined for holes specifically, and could differ for electrons. Unipolar injection is strongly implied by the sub-band gap applied bias. The sign of the charge carriers, plus additional evidence for unipolar injection, is demonstrated by ammonia compensation experiments. Exposure of a biased sample under vacuum to ammonia vapor for two minutes demonstrated a sharp drop in both current and NIR absorbance (Figure 2.8). Ammonia compensation is known to selectively compensate p-type carriers,[79] and the significant absorbance change in particular identifies the great majority of the carriers as p-type. Although it is possible to n-dope this polymer[93], the position of the electrode edge close to the valence band, combined with the low applied bias, is consistent with this result.

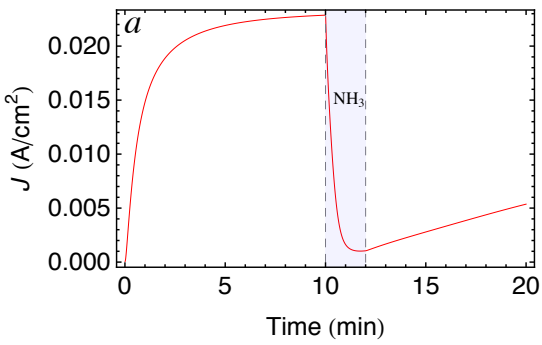

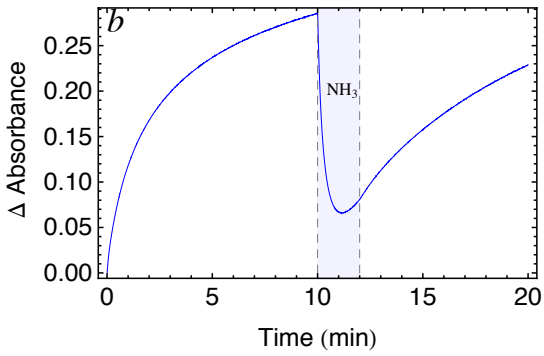

Figure 2.8. Current (a) and absorbance change at 1060 nm (b) for a film exposured to ~200 torr dry ammonia vapor. 1.5 V bias is applied constantly, and the exposure is followed by vacuum.

2.3.2. Determining the Diffusion Coefficient

With our understanding of charge injection, transport through the material can be modeled with greater certainty than would otherwise be possible. In particular, the measured qd_h and J may be used to calculate the diffusion coefficient so long as we are assured of unipolar injection and complete screening of the applied field in the bulk. The first condition has been explicitly addressed above. The second condition is consistent with electrochemically supported charge injection, as demonstrated by the charge-voltage relationship shown in Figure 2.7. Furthermore, the Debye length characterizing an ion concentration of $\sim 1 \times 10^{21}$ cm^{-3} is < 0.1 nm. The Debye length calculated on account of the electronic carriers alone ranges from 5 nm to < 0.5 nm at the highest concentration, for a 479 nm thick device. These factors strongly suggest that any applied field would be screened close to respective electrodes. The model of charge injection indicated by these measurements is illustrated in Figure 2.9.

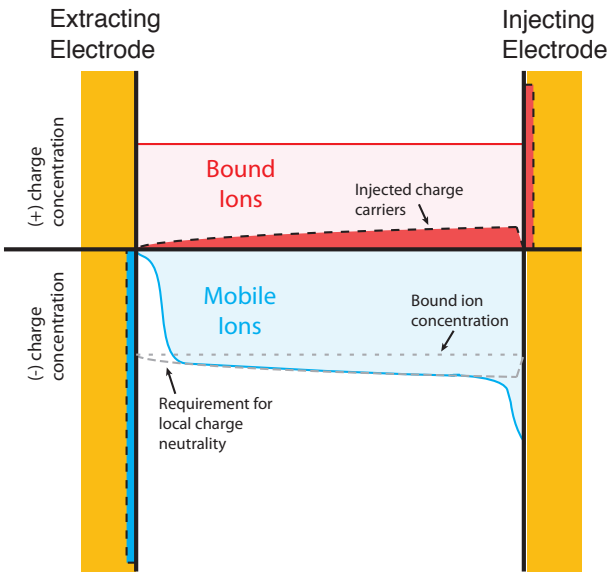

Figure 2.9. Concentrations of positive and negative ions and charge carriers across the film and electrodes. Through the bulk of the film, injected holes are compensated by movement of a much higher concentration of pre-existing negative ions. Total charge neutrality is achieved by compensating charges on the extracting electrode.

Variations on this model of electrochemically supported charge injection have been previously suggested for this,[59,75] and other[56,89,95,96] conjugated polyelectrolyte systems. The high relative ion concentration also means that the ionic depletion layer generated near the extracting electrode will not reach substantially into the bulk. Based on the ion concentration relative to the measured injected charges, the ionic depletion region is estimated to extend only 6% of the device thickness at the highest levels of injection. As indicated by the charge-voltage behavior, transport in this system is taken to be bulk, rather than injection limited. However, so long as the conditions of screened fields and unipolar injection apply, the following calculation of diffusion coefficient is valid for either case.

With the electric field screened by ion movement, the flux of carriers F across the sample at steady state will be governed by diffusion as follows:

$$F = -D\frac{dn_h}{dx} \quad \text{or} \quad J = -qD\frac{dn_h}{dx} \quad (5)$$

Where D is the diffusion coefficient, n_h is the concentration of carriers, J is the current density, and q is the elementary charge. If D does not vary as a function of concentration, the carrier profile will be linear across the thickness of the sample. From this observation, the concentration gradient can be easily obtained from d_h and the sample thickness L.

$$\frac{dn_h}{dx} = \frac{2d_h}{L^2} \quad (6)$$

Combining Eqs. 5 and 6 and rearranging for the diffusion constant yields

$$D = \frac{-JL^2}{2qd_h} \quad (7)$$

According to Eq. 7, when the extinction coefficient ε is applied to ΔA to obtain d_h, it should display a linear relationship with J. However, as shown in the power-law plot of Figure 2.10, the increase in J far outstrips that of d_h. This is indicative of a concentration-dependent D.

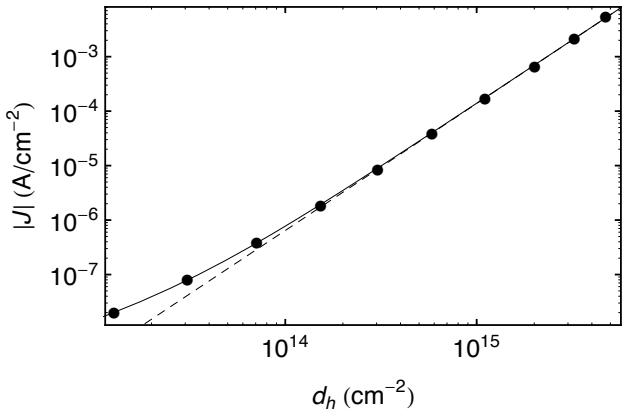

Figure 2.10. Current density as a function of carrier density, as determined by NIR absorbance, for a series of applied biases (•). The dashed fit assumes a concentration-dependent diffusion coefficient alone (Eq. 8), while the solid fit includes a concentration-independent element (Eq. 14).

The slight curvature evident in the low-concentration region of Figure 2.10 suggests the influence of a small concentration-independent component of D, representing the diffusion coefficient of a solitary carrier. This term is expected, as otherwise the mobility in the infinite-dilution limit would be zero. At higher concentrations, the apparent dominance of the concentration-dependent term allows us to neglect any concentration invariant terms and consider the diffusion as $D=\beta c$. Additionally, the apparent power dependence of the observed J shown in Figure 2.10 suggests that it is appropriate to expand this to:

$$D = \beta\left(\frac{c}{C_0}\right)^{\gamma} \quad \text{or} \quad D = \beta\left(\frac{n_h q}{C_0}\right)^{\gamma} \qquad (8)$$

where c is the charge concentration, and C_0 is a reference concentration of 1 C/cm^3. Alternately this may be expressed in terms of n_h. A power dependence of diffusion on concentration is the simplest mathematical fit to the observed behavior, and it is also consistent with conduction by variable-range hopping which is commonly observed in conjugated polymers.[97-101]

This form of concentration dependence now enables a more accurate picture of the charge profile across the device and its relation to current. Substituting Eq. 8 into 5 and integrating over the position x we may derive the flux, and the concentration as a function of x, with the boundary condition that the hole concentration is 0 at the extracting electrode (x=0).

$$F = \frac{-\beta}{x(\gamma+1)}\left(\frac{q}{C_0}\right)^{\gamma}\left[n_h(x)\right]^{\gamma+1} \quad (9)$$

$$n_h(x) = \left(\frac{-F(\gamma+1)}{\beta}\left(\frac{q}{C_0}\right)^{-\gamma} x\right)^{\frac{1}{\gamma+1}} \quad (10)$$

This concentration may in turn be related to d_h by integrating $n_h(x)$ over the length L of the sample

$$d_h = \int_0^L n_h(x)dx \quad (11)$$

Substituting from Eq. 10 and solving, we may solve for $n_h(L)$, the concentration at the injecting electrode.

$$n_h(L) = \frac{d_h}{L}\left(\frac{\gamma+2}{\gamma+1}\right) \quad (12)$$

Evaluating the flux Eq. 9 at length L, substituting $n_h(L)$ from Eq. 12 and solving for current density yields:

$$J = -\beta\left(\frac{qd_h}{LC_0}\right)^{\gamma+1}\frac{C_0(\gamma+2)^{\gamma+1}}{L(\gamma+1)^{\gamma+2}} \quad (13)$$

Eq. 13 shows that the power dependence of J on the measured d_h may be used to extract the value of γ and, using that result and the magnitude of the current density, β. As discussed previously, this approach is suitable for higher carrier concentrations, where the dependence of current follows a power law (see Figure 2.10). Applying Eq. 13 to our results from 0.8 - 1.4 V, the value of β is 4.42×10^{-10} cm^2/s and γ is 1.3. After determining the concentration-dependent term by this method, the concentration-independent term may be considered by treating diffusion as:

$$D = \alpha + \beta\left(\frac{c}{C_0}\right)^{\gamma} \quad (14)$$

Solving this form for flux,

$$F = \frac{\alpha n_h(x)}{x} - \frac{\beta}{x(\gamma+1)}\left(\frac{q}{C_0}\right)^{\gamma}\left[n_h(x)\right]^{\gamma+1} \quad (15)$$

This enables numerical determination of the charge profile (Figure 2.11) and, integrating across x, the total d_h. This plot demonstrates that for at low J values, corresponding to bias below 0.7 V, inclusion of the concentration-independent α term requires considerably decreased charge injection to support the observed current. However, for values of J corresponding to higher bias, the two models are indistinguishable.

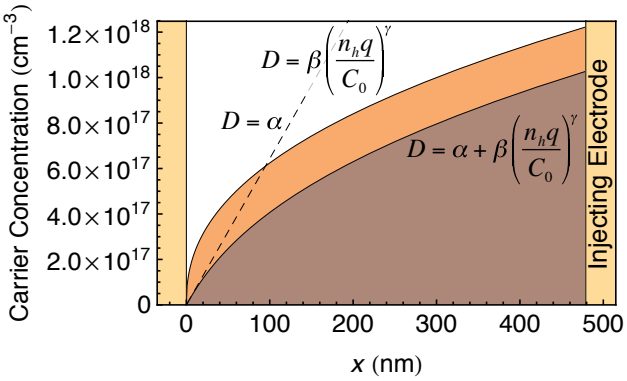

Figure 2.11. Calculated charge concentration profiles between the electrodes for a given current (that resulting from an applied bias of 0.6 V), including (brown, Eq. 14) and neglecting (orange, Eq. 8) the concentration-independent term α.

Using the previously determined values of β and γ, α may then be determined by fitting to the J/d_h values at low concentration. The values of hole diffusion and mobility (from the Einstein relation) thus determined are:

$$D = 7.8 \times 10^{-12} + 4.4 \times 10^{-10}\left(n_h q / C_0\right)^{1.3} \text{ cm}^2/\text{s}$$

$$\mu = 2.8 \times 10^{-10} + 1.6 \times 10^{-8}\left(n_h q / C_0\right)^{1.3} \text{ cm}^2/\text{Vs}$$

Across the measured range of concentrations, the calculated mobility varies between 5×10^{-10} and 5×10^{-7} cm^2/Vs (see Figure 2.12).

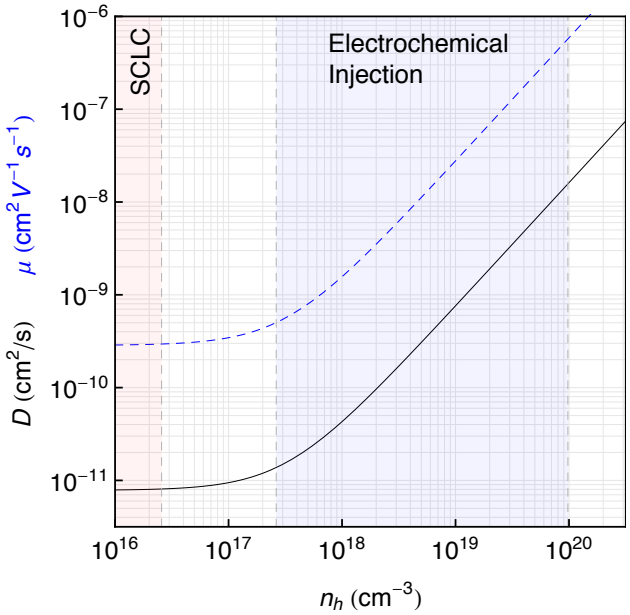

Figure 2.12. Calculated diffusion coefficient(—) and mobility (---), plotted as a function of concentration. The blue region represents the concentration range accessed in this study, while the red region demonstrates the concentration range accessible by SCLC methods.

This mobility is lower than that reported for many polyacetylenes, but this is unsurprising given that previous characterization suggests that the morphology is

amorphous. Considering that local carrier concentration is balanced by excess anions, it might be tempting to suggest that the observed concentration dependence resulted from ion, rather than carrier concentration. However, considering the high intrinsic concentration of ions, it is apparent that the relative anions concentration varies only marginally across the film (see Figure 2.9). The mobility may well depend on ion concentration, yet it is clear that the strong dependence observed in this study corresponds to carrier concentration instead.

In organic semiconductors, a power-law dependence of *conductivity* on concentration is often interpreted as originating from variable-range hopping between a distribution of trap states.[97-102] It is readily apparent that a power-law dependence of conductivity of concentration correlates with a similar relation for mobility, with the associated power being one less.[73] Reported values for the power dependence of mobility in other organic semiconductors range between 0.9 and 4,[73,97,99,101] consistent with our measured value of 1.3. Figure 2.12 also demonstrates the importance of ion polarization-assisted charge injection when characterizing the mobility in conjugated polyelectrolyte systems. The red region in this figure demonstrates the calculated concentration range that would have been generated purely by space-charge limited injection (using short pulses of bias up to 11 V).[71] This suggests that even if the SCLC regime of conduction could have been accessed in this manner, it would have been well into the concentration-independent range of mobility, preventing accurate characterization of the concentration dependence.

2.3.3. Release of Injected Charge

While the above analysis relies on NIR absorbance to provide the necessary quantification of charge injection, the experimental procedure included another approach to obtaining this same information. After a given applied bias, the sample was allowed to relax back to its initial state under short circuit for 8 hours. The current discharged through this short circuit, divided by the device area (J_{SC}) was recorded along with the absorbance (Figures 2.13a and b). The integration of post-bias discharge has previously been used to quantify charge injection into conjugated systems with mobile ions.[34] When a system with injected charges is short-circuited there are two paths by which the charges may recombine. They may pass through the external circuit, or they may recombine internally (in a system with unipolar injection, recombination occurs between the charges injected into the semiconductor and compensating charges on the opposite electrode). Only the external discharge is actually observed by measurement of J_{SC}. In the aforementioned analysis, it was argued that the relative impedance across the sample vs. the external circuit makes the undetected internal recombination a negligible source of error. The simultaneous measurement of short-circuit current together with the quantification of injected charge through absorbance allows us to test this supposition in our system.

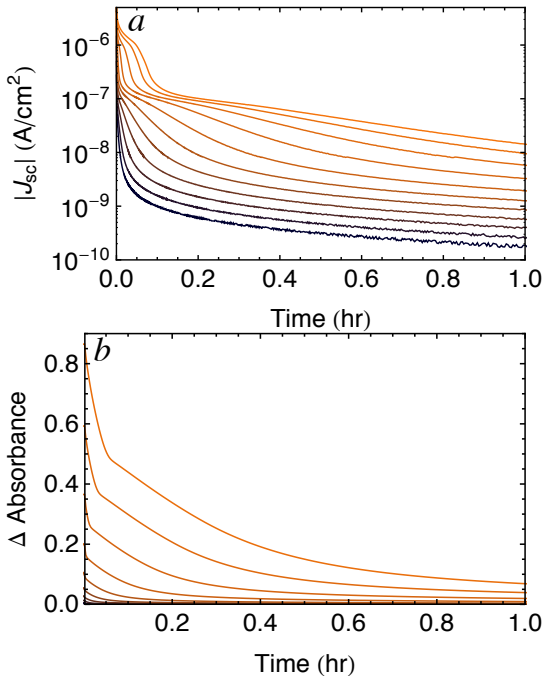

Figure 2.13. Short-circuit current (a) and absorbance change (b) following bias steps from 0.5 V to 1.4 V.

In both measurements two distinct rates of discharge are observed. One, taking place over several hours, is present in all measurements. The other, which occurs over a faster timescale, is only observed following bias exposures above ~1 V.

Integrating the short-circuit currents to obtain the d_h, we may compare these result to the charge injection by absorbance for the same scans. The ratio of these (Figure 2.14) equals the fraction of the total charge that recombined through the external circuit. The greater than 100% charge observed for 0.5 - 0.7 V is readily explained by another weakness of the short circuit discharge method: it does not distinguish between injected charge and interfacial ionic capacitance. Absorbance, on the other hand, measures only carriers in the conjugated system and is blind to

charge stored on the electrodes. At higher biases, where the exponentially dependent injection of charge greatly exceeds the interfacial capacitance, the methods may be better compared, and it is indicated that approximately 65% of injected charge recombines through the external circuit. This branching ratio is consistent with previous numerical modeling of diffusive decay of a linear charge concentration profile.[75]

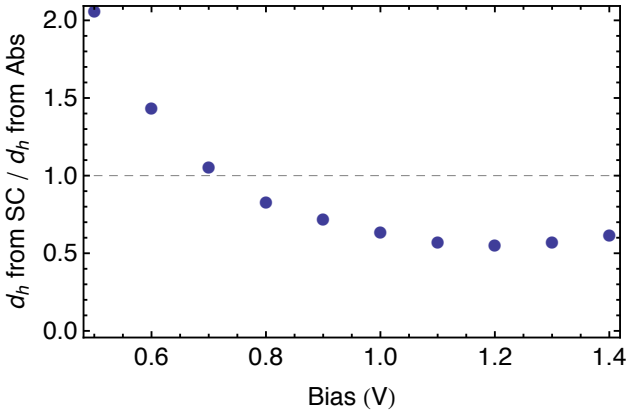

Figure 2.14. The fraction of charge (measured by absorbance) which is observed when integrating the short-circuit discharge current.

Using the time derivative of the d_h from absorbance, we obtain the total recombination current density ($J_{discharge}$) as a function of time. Dividing the measured J_{SC} by $J_{discharge}$, we observe how the much of the charge is recombining through the external circuit at any given moment (Figure 2.15).

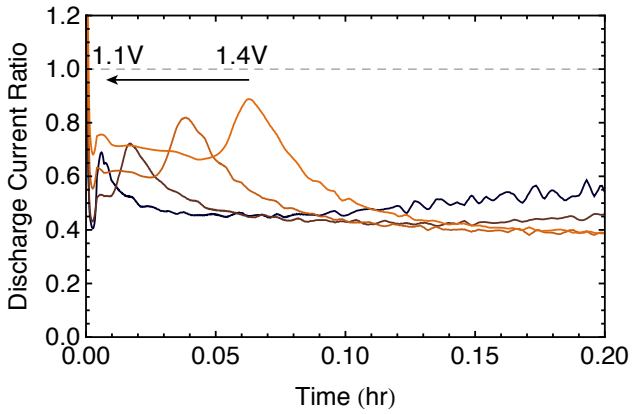

Figure 2.15. Short circuit current divided by the total recombination current from the derivative of d_h.

Following low bias periods, the rapid decay of absorbance makes the derivative of d_h unusable. As the bias is increased, decay occurs over a longer period, and the interfacial ionic capacitance is rendered negligible, revealing more interesting behavior from the decay of injected charges. Specifically, the proportion of charges released through the external circuit displays a peak at some intermediate time, rising to 90% following 1.4 V bias. The position of this peak in time corresponds to the transition between the initial, rapid decay and the more gradual decay that follows (see Figure 2.13a and b). Following this peak, the ratio falls off to ~50%.

That the injected charge does not discharge solely through the low-impedance external circuit should not be surprising. Nor should it be surprising that the balance of recombination by internal and external routes displays complex behavior over time. The external circuit is indeed much lower impedance than the internal, but at the moment of short circuit, some portion of the injected charge

begins closer to the extracting electrode than to the injecting electrode (see Figure 2.11). Additionally, while the distribution of charges favors diffusion primarily through the injecting electrode (and the external circuit), the ions which screen the field under bias exert their own field under short circuit. This field may initially serve as a barrier to extraction from the injecting electrode.

2.4. Conclusion

In conjugated polymers featuring soliton or bipolaron charge injection bands, direct quantification of charge injection by NIR absorbance spectroscopy provides significant assistance in the determination of mobility. With this measurement, the mode of charge injection and transport may be determined with considerably greater confidence. Additionally, separate quantification of charge density enables the determination of mobility where the presence of screening ions would prevent these measurements by time-dependent or steady-state *J*-*V* measurements alone. Finally, in the case of concentration or field-dependent mobilities, the addition of a third measured parameter is vital.

In intrinsic organic semiconductors, measurement of charge injection by absorbance is a technique well suited to conjugated polyelectrolytes or other systems with mobile ions, where ion-assisted injection supports charge densities sufficient to be readily observable. The method of mobility determination demonstrated in this study may be used so long as unipolar charge injection

predominates, the mobile ions have sufficient density to screen the applied field, and the extinction coefficient of the primary charge carrier can be determined. If the diffusion coefficient displays a concentration dependence, its form may be inferred from the current/charge density relationship over a range of biases, and this relationship can in turn be used to derive a carrier concentration profile across the sample. For the PA_C used in this example, the data was fit with a power law concentration-dependent diffusion coefficient, although straightforward solutions were also supplied for concentration-independent diffusion coefficients. The power-law concentration dependence observed is consistent with the variable-range hopping model commonly applied to disordered semiconductors. The prevalence of organic semiconductors displaying this strong concentration dependence highlights the importance of measuring carrier concentration when attempting to determine mobility.[74]

Independent quantification of carrier concentration, combined with a measurement of short-circuit current, also enables a more detailed analysis of the fate of injected charges during relaxation. Crucially, it also allows us to judge the efficacy of integrated short-circuit current as a measure of injected charge. While we have stated before[75] that short-circuit current serves as a lower limit for the quantity of injected charge, our measurements show that at low levels of injection, interfacial ionic capacitance can actually result in overestimation of injected charge. At higher levels of injection, it is demonstrated that integrated short circuit current is sufficient as a rough estimate of injected charge density. The factors governing internal vs. external recombination are not currently well understood, but the use of

carrier quantification by absorbance might reveal a predictable branching ratio. Were this the case, integrated short circuit might come to serve as a reliable technique where carrier quantification by absorbance is not an option.

2.5. Bridge to Chapter III

Chapter II has demonstrated the importance of gaining a third measurable parameter, in addition to J and V, when attempting to make quantitative measurements of the fundamental material parameters in MIEC systems. In particular, quantifying d_h through NIR absorbance has proved to be extremely valuable. Measuring charge injection not only assists in the assignment of material parameters such as D and μ, it also gives us greater confidence in constructing detailed qualitative models of the internal dynamics of MIEC systems. This is important, because when considering the conduction of an isolated MIEC in the *unipolar* regime, we step outside the body of understanding built up by the extensive study of PLEC's, which necessarily operate in bipolar injection regime. The matter of charge neutrality now gains new importance, and the mechanism we proposed to resolve this issue in chapter II makes some surprising and potentially important predictions about the behavior of MIEC's in the context of other device architectures. In chapter III, we will explore these predictions, constructing a more precise model of how MIEC's in the unipolar injection regime interact with their electrodes, and testing this model in an experimental system.

CHAPTER III

EXTRACTING-ELECTRODE SPACE-CHARGE LIMITED CURRENT: CONJUGATED POLYELECTROLYTES WITH SEMICONDUCTING CONTACTS

This chapter contains material that is to be submitted for publication in the Journal of Physical Chemistry Letters. I performed the experiments and analysis, with helpful discussion and editorial oversight by Mark Lonergan

3. 1. Introduction

In the field of organic semiconductors, increasing attention is being paid to materials containing mobile ions.[64,65] Whether in the form of conjugated polyelectrolytes, or blends of solid electrolyte and semiconductor, mixed ionic-electronic conductors (MIEC's) are displaying their utility in a number of different applications. Promising roles for these materials include the active material in

organic light-emitting electrochemical cells,[103] organic field-effect transistors,[37,38] and carrier selective injection layers in organic photovoltaics or light emitting devices.[44,70] However, attempts to incorporate these materials into existing device architectures are unlikely to succeed unless their unique properties are taken into account. Some of these properties, such as current-voltage behavior which is time-variant on the scale of minutes or more, have been recognized and thoroughly explored.[75] It has also been shown that the presence of mobile ions has a significant influence on the electronic behavior of semiconductor – electrode interfaces. For instance, a well-known characteristic of MIEC's is significantly enhanced carrier injection relative to the equivalent non-ionic semiconductor.[58,59,104] Two processes are responsible for this enhancement. Firstly, the accumulation of ions at the injecting electrode compresses any existing barrier to carrier injection, increasing tunneling. Additionally, a process similar to electrochemical doping enables the compensation of a vastly increased carrier concentration in the bulk.

Herein, we demonstrate that the same ion redistribution processes understood to be responsible for enhanced charge injection into MIECs also lead to some unexpected and previously unrecognized interactions with other conducting materials in the system. Specifically, we test the hypothesis that unipolar charge injection into an MIEC can be limited by the capacity of an appropriate carrier-*extracting* semiconductor electrode to support space charge. By appropriate, we mean a p-type semiconductor for hole transport and an n-type semiconductor for electron transport. In these situations, the interface region of the semiconductor near the MIEC will be in depletion when acting as the extracting electrode and in

accumulation when acting as an injecting electrode. We hypothesize that this difference will lead to asymmetry in the amount of charge that can be injected into the MIEC with applied bias, and thus to current rectification. When the semiconductor acts as the injecting electrode and is under accumulation, there is little difference from a metal electrode. When the semiconductor acts as the extracting electrode and is under depletion, however, the level of charge injection into the MIEC is limited because a large fraction of the applied bias goes into supporting the charge depletion layer in the semiconductor and hence is not available to drive charge injection into the MIEC (see Figure 3.1).

It has not been intuitive, nor has it been previously recognized in the literature, that the capacitance of the extracting electrode interface may dominate the electrical behavior of MIEC systems, and lead to unexpected current rectification. This phenomenon, which we here describe as extracting-electrode space-charge limited current (EE-SCLC) may be relevant wherever a MIEC is interfaced with a semiconductor. Applications where EE-SCL conduction might dominate include the incorporation of conjugated polyelectrolytes as injection layers for OPV[49] or perovskite solar cells, or as the active layers in electrolyte-gated transistors.[37,38]

EE-SCL is here described in a quantitative model and experimentally demonstrated by the electrical behavior of a conjugated polyelectrolyte (see chapter 2, Figure 2.1) on a p-type silicon substrate.

3.2. Experimental

PA_C (see Figure 2.1, chapter 2) was synthesized by a ring-opening metathesis polymerization of the cationically functionalized cyclooctatraene.[67,87] Thin-films were fabricated by spin-coating in air out of a 10mg/ml solution of polymer in DMF onto B-doped p-type Si with a resistivity of 0.1-0.3 Ω cm. Before deposition a thin drop of epoxy was cured on the Si to serve as an insulating platform for top electrode lead, and the thin-film was deposited such that it extended over the edge of the epoxy. Oxygen exposure was restricted to several minutes before the evaporation of a masked 15 nm top gold contact. The sample was annealed under vacuum at 125° C for 8 hours to expel bound oxygen and DMF. *J-V* and absorbance measurements were then performed under vacuum on a temperature-controlled chuck (see Figure 2.2), where the sample was held at 45° C to enhance ion conductivity. Electrical measurements were performed using an Agilent 4156C parameter analyzer. Using a monochrometer with a tungsten halogen light source, a probe beam was focused within the 0.112 cm^2 sample area, and subsequently measured using an InGaAs detector in short-circuit mode. The Si substrate was both-side polished so as to not diffuse the transmitted light. The measured transmittance was corrected for the simultaneously measured light source intensity.

3.3. Results

3.3.1. EE-SCLC Model

We begin by describing a quantitative model, which demonstrates EE-SCLC by treating the carrier concentration and electrostatic potential across a mixed ionic-electronic conductor (MIEC) system (Figure 3.1), and predicting the resulting current density-voltage (J-V) behavior.

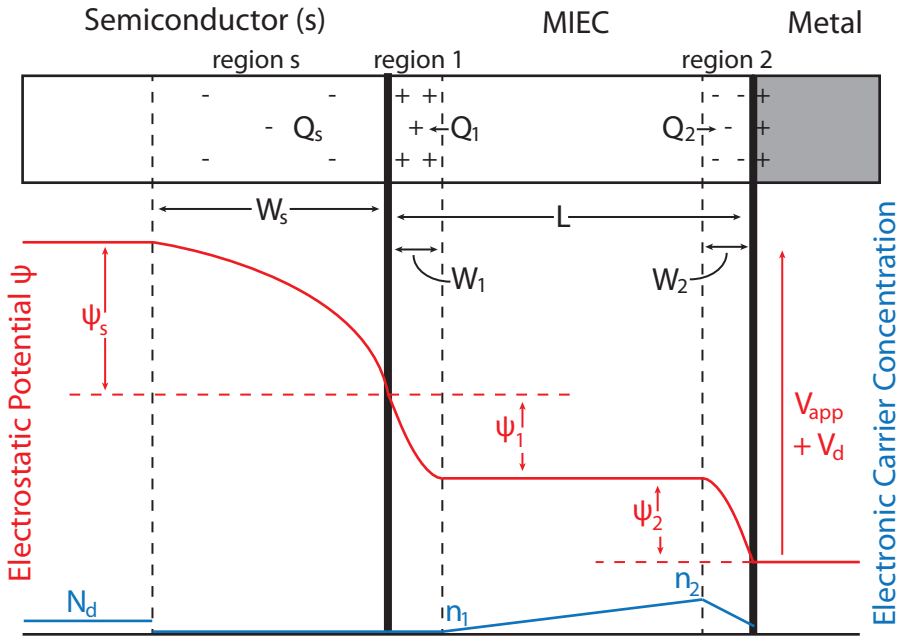

Figure 3.1. A profile of an MIEC contacted by a semiconductor on one side and a metal on the other. Electrostatic potential ψ (red) and electronic carrier concentration n (blue) are shown for an applied bias driving hole injection from the metal. This corresponds to "reverse bias" in the EE-SCLC system. The diagram for an electron-conducting MIEC system would be similar except for an inversion of ψ and the sign of charge regions. The accumulation and depletion widths W_s, W_1 and W_2 are exaggerated for clarity.

The system is divided into three parts: (1) an MIEC with mobile ion concentration c_o, is in the center; (2) a metal electrode contacted to the MIEC on one side; and (3) a semiconductor electrode with dopant concentration N contacted to the MIEC on the other side (see Figure 3.1). The metal and semiconducting electrode are considered to be ion blocking. We consider the unipolar hole injection regime, which is expected when the Fermi levels of the contacts are significantly nearer the valence band edge than the conduction band edge of the MIEC. This corresponds to a high work function metal and p-type semiconductor for the electrodes. The model applies equally to electron injection from low work function/metal electrodes by simply reversing the sign of bias. In either case, the electrodes are considered blocking to ions. Under applied bias, ion mobility leads to regions of excess charge in the MIEC near the semiconductor (region "1") and metal (region "2") interfaces. These charge regions are in turn coupled to opposite regions in the adjacent metal (region "m") and semiconductor (region "s"). Each of these regions has an associated potential drop (ψ_x), width (W_x), and a total excess charge (Q_x) where x is used to denote the region. The fraction of the total applied bias dropped across a given region is expressed as f_x.

Below is detailed an approach wherein we model the current through the MIEC from the carrier profile, which is in turn determined by the surface concentration of carriers at the respective electrode interfaces. These concentrations are modeled by the Nernst equation. Potential drops, including those across the MIEC diffuse layers, are determined by treating the system as a series of coupled capacitors; the capacitance of the semiconductor under depletion

is determined by the abrupt-layer approximation, while capacitances of the MIEC diffuse layers and the semiconductor under accumulation are modeled by the Guoy-Chapman theory. The effect of initial Fermi-level offsets and the resulting built-in potentials are also accounted for in this model.

Steady-state electronic current across the MIEC is given by

$$J = qD\frac{n_2 - n_1}{L} \quad (1)$$

where J is the current density, D is the diffusion coefficient of electronic carriers, n_1 and n_2 are the concentrations of electronic carriers in the MIEC adjacent to the semiconductor and metal interfaces (just inside the diffuse layer), and L is the MIEC thickness. Equation 1 assumes that the Debye length of ions in the MIEC is a small fraction of L and that D is concentration independent. The first of these assumptions implies complete screening of the electric field in the bulk, so this is necessarily a diffusive transport model. Concentrations n_1 and n_2 are determined by V_{app}, f_1 and f_2, and by the Nernst equation:

$$n_1 = n_0 \exp\left[\frac{f_1 \overline{V}_{app}}{\Omega}\right] \quad (2)$$

$$n_2 = n_0 \exp\left[-\frac{f_1 \overline{V}_{app}}{\Omega}\right] \quad (3)$$

where n_o is the electronic carrier concentration at zero bias, and Ω is a constant factor relating to the density of states of the MIEC. It is the reciprocal of the classic "n" term in the Nernst-equation indicating the stoichiometric number of electrons

involved in an electrode reaction. Here, it can be less one (Ω>1) reflecting a density of states profile that is broadened relative to a simple small molecule, one-electron redox couple, as is typical for conjugated polymers.

In the absence of initial Fermi level offsets between the MIEC and semiconductor, $f_1 V_{app} = \psi_1$ and $f_s V_{app} = \psi_s$. Otherwise, the potential drop across the semiconductor/MIEC interface may be related to applied bias as follows:

$$\bar{\psi}_1 = f_1 \bar{V}_{app} + \bar{\psi}_{1o} \quad (4)$$

$$\bar{\psi}_s = f_s \bar{V}_{app} + \bar{\psi}_{so} \quad (5)$$

Where Δ_s, the total Fermi level offset between the semiconductor and MIEC at V_{app} = 0, is split between the MIEC and semiconductor:

$$\bar{\Delta}_s = \bar{\psi}_{1o} + \bar{\psi}_{so} \quad (6)$$

Potential and voltage values are here expressed as a reduced quantity, where $\bar{x}$ denotes $\bar{x}/V_t$, where V_t is the thermal voltage kT/q.

From equations 1, 2 and 3, it is apparent that the current is dependant on f_1 and f_2. The value of these parameters can be determined using the following assumptions: (1) The capacitance of the metal electrode is considerably greater than the other interfaces, so $f_m \approx 0$. (2) Ion polarization in the MIEC is symmetric, which means that $f_1 = f_2$, and, together with the previous assumption, that

$$2f_1 + f_s = 1 \quad (7)$$

(3) There is overall charge neutrality, and (4) That the total injected electronic carriers are negligible relative to the excess charge due to ion polarization, which together with the previous assumptions means that

$$Q_s = -Q_1 = Q_2 = -Q_m \quad (8)$$

(5). The charge in the semiconductor electrode under depletion Q_{sd} and its relation to the electrostatic potential drop in this region ψ_s is given by the abrupt layer approximation:

$$Q_{sd} = qNW_s = qN\sqrt{\frac{2\varepsilon_s\psi_s}{qN}} \quad (9)$$

where q is the elementary charge and ε is the dielectric constant. (6) The relation between the semiconductor charge under accumulation Q_{sa} and ψ_s, as well as the relations of Q_1 and Q_2 to ψ_1 and ψ_2 in the MIEC are given by with the low-ψ limit of the Guoy-Chapman theory:

$$Q_x = \frac{\varepsilon_x}{\lambda_x}\psi_x \quad (10)$$

where λ_x is the Debye length of the material in region x:

$$\lambda_i = \sqrt{\frac{\varepsilon_x kT}{c_x q^2 \Sigma}} \quad (11)$$

where c_x is the salt concentration, or the dopant concentration in a semiconductor, and Σ is the sum of the square of the charge number Z for the mobile charge carriers in the system (1 for a monovalent salt with one fixed ion, 2 for a similar salt where

both ions are mobile). Equations 9, 10 and 11 may be combined and simplified to give the relation between charge and potential drop in these regions:

$$Q_{sd} = \sqrt{\bar{\psi}_s}\sqrt{2qN\varepsilon_s V_t}$$
$$Q_{sa} = \bar{\psi}_s\sqrt{qN\varepsilon_s V_t}$$
$$Q_1 = \bar{\psi}_1\sqrt{qc_o\varepsilon_1 V_t\Sigma} \quad (12, 13, 14)$$

These expressions may be used, in conjunction with equation 8, to determine the relation between ψ_s and ψ_1, depending on whether the semiconductor is in accumulation or depletion.

$$\bar{\psi}_s = \gamma\bar{\psi}_1^2 : \psi_1 > 0$$
$$\bar{\psi}_s = \left(\sqrt{2\gamma}\right)\bar{\psi}_1 : \psi_1 < 0 \quad (15, 16)$$

where γ relates the capacitance of the MIEC with that of the semiconductor under accumulation:

$$\gamma = \frac{\varepsilon_1 c_o \Sigma}{2\varepsilon_s N} \quad (17)$$

If the Fermi level of the isolated MIEC and semiconductor are identical, then the semiconductor will be driven into depletion when V_{app} is positive, and accumulation when it is negative. If instead there is a Fermi level offset Δ_s, then equilibration between semiconductor and MIEC will induce potential drops in the semiconductor and MIEC at zero bias (see equation 6), pushing the semiconductor into depletion or accumulation at $V_{app} = 0$. As a result, it would require an external bias, designated V_d if the semiconductor starts in depletion, and V_a if it starts in accumulation, to return

ψ_s and ψ_1 to 0 (See figure 3.2). Note that due to ion polarization in region 2 at the metal electrode, $|V_d\ ,\ V_a\ | > |\Delta_s|$.

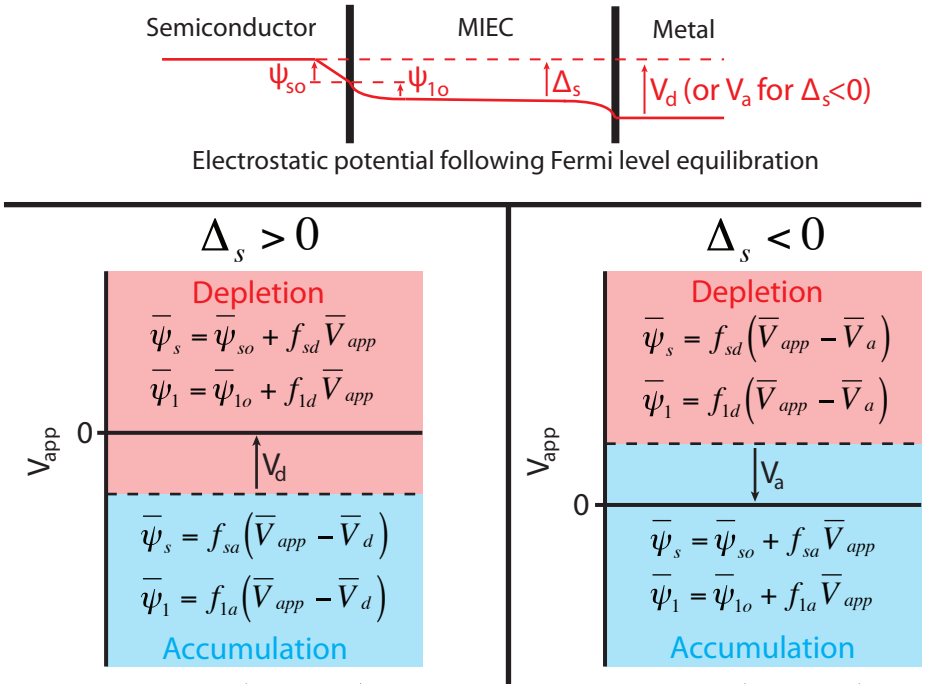

Figure 3.2. Top: the electrostatic potential at zero bias following Fermi level equilibration. The system shown exhibits a positive Fermi-level offset between MIEC and semiconductor Δ_s. Total built-in voltage V_d or V_a is shown on the right. Bottom: Determination of ψ_s and ψ_1 depends on the sign of Δ_s, and also on whether the V_{app} under consideration drives the semiconductor into accumulation (f_{1a}) or depletion (f_{1d}). Note that the division between depletion and accumulation is offset from 0 V by V_d or V_a. Calculations for f_{1a}, f_{1d} and V_d or V_a for these cases are given below.

$$f_{1a} = \frac{1}{2}\left(\frac{1}{1+\sqrt{\gamma/2}}\right)$$

$$f_{1d} = \frac{1}{1-\gamma\left(\overline{\Delta}_s + \overline{V}_d\right) + \sqrt{1+\gamma\left(\overline{V}_{app} - \overline{V}_d\right)}}$$

$$\overline{V}_d = -\left[\overline{\Delta}_s + \frac{1}{2\gamma}\left(\sqrt{1+4\overline{\Delta}_s\gamma} - 1\right)\right]$$

(18, 19, 20)

$$f_{1a} = \frac{1}{2}\left(\frac{1}{1+\sqrt{\gamma/2}}\right)$$

$$f_{1d} = \frac{1}{1+\sqrt{1+\gamma\left(\overline{V}_{app} - \overline{V}_a\right)}}$$

$$\overline{V}_a = -\overline{\Delta}_s\left(1 + \frac{1}{1+\sqrt{2\gamma}}\right)$$

(18, 21, 22)

V_d or V_a marks the transition between accumulation and depletion in the case of Fermi level offset, and enables the f_1 and f_s to be treated piecewise in terms of V_{app}.. If Δ_s is neglected, f_1 may be simplified to:

$$f_{1a} = \frac{1}{2}\left(\frac{1}{1+\sqrt{\gamma/2}}\right) \qquad f_{1d} = \frac{1}{1+\sqrt{1+\gamma\overline{V}_{app}}} \qquad (23, 24)$$

In this manner, injected carrier concentration, which is dependent on $f_1 V_{app}$ (equations 2 and 3) may be determined as a function of V_{app}. If D is known, than J/V behavior may be predicted also (equation 1). Note the dependence of f_1 on γ; when the capacitance of the extracting electrode is much greater than that of the MIEC, γ approaches 0 and f_1 approaches 1/2 under either sign of bias. However, when the extracting electrode has a much lower capacitance, $f_1 < 1/2$ under both signs of bias, but voltage dependant when the semiconductor is under depletion (equation 24). In this case the increasing fraction of V_{app} dropped across the semiconductor under positive bias to the metal results in suppressed carrier injection and the emergence of current rectification (see Figure 3.3). This is the characteristic J/V behavior of EE-SCLC.

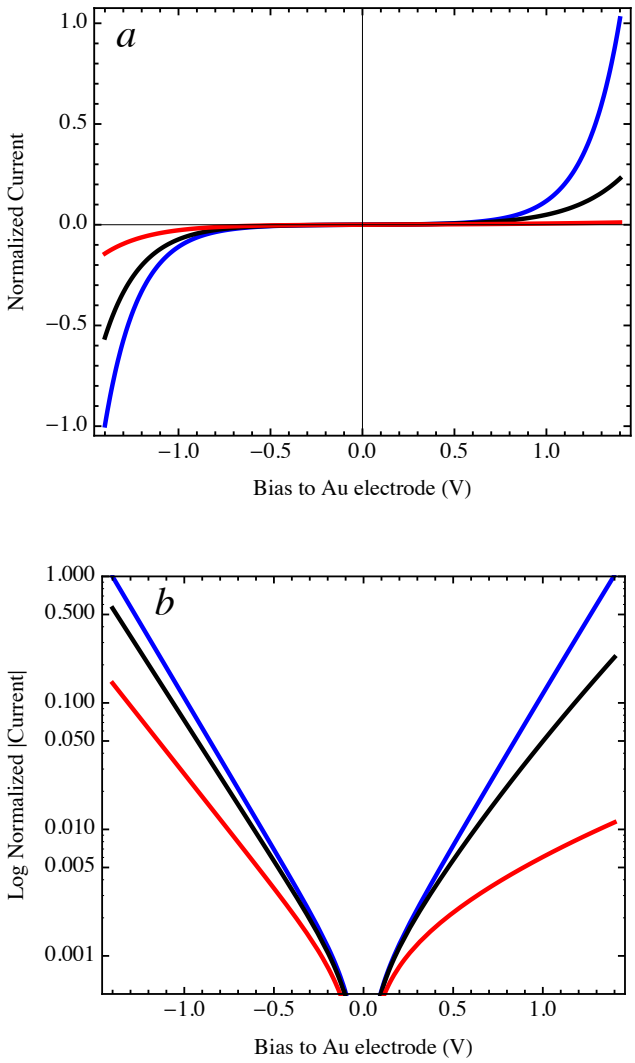

Figure 3.3. Relative current density (a) and log current density (b) predicted using the EE-SCLC model for three different values of γ: 0.003 (blue), 0.03 (black), and 0.3 (red). The other parameters used are constant: $\Omega = 3$ and $\Delta_s = 0$. J is taken to be proportional to n_i (constant D). Note that both forward (negative) and reverse (positive) current are attenuated by the increasing ratio of MIEC : semiconductor capacitance, but that reverse bias is most strongly affected, leading to current asymmetry.

We may also consider the quantity of electronic carriers injected into the MIEC, expressed as d_h (with units of h^+/cm^2). When the diffusion coefficient of electronic

carriers has a constant value, the carrier profile will be linear, and d_h will be given by

$$d_h = n_e L + \frac{(n_i - n_e)L}{2} \quad (25)$$

where n_i is the carrier concentration at the injecting electrode and n_e the concentration at the extracting. If the latter is negligible, this reduces to

$$d_h = \frac{n_i L}{2} \quad (26)$$

in which case, d_h will scale proportionally with $|J|$. However, if D is concentration dependant (see Figure 3.4), then equations 1 and 26 are no longer valid. In this instance, $|J|$ and d_h are no longer proportional. Note that the rest of the model is unchanged, and that n_i is still governed by $f_1 V_{app}$ according to equations 2 and 3. The relation between n_i and J will now depend on the specific concentration dependence of D, as will the relation between n_i and d_h. However, the latter relation may be bounded within a factor of two:

$$n_i L > d_h > \frac{n_i L}{2} \quad (27)$$

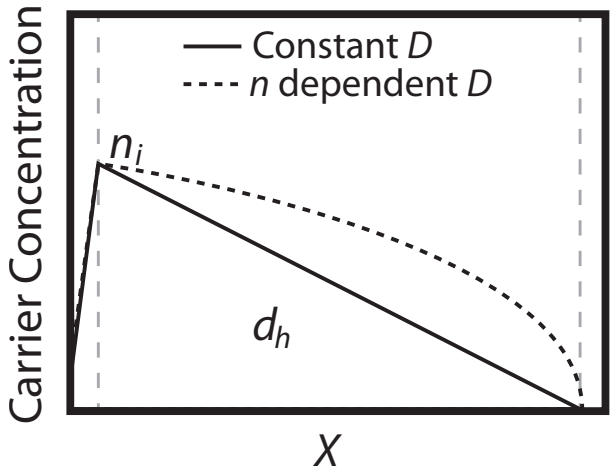

Figure 3.4. Electronic carrier profiles across the length of the MIEC (injection on the left) for constant D (—) and power-law dependent D (---). The integrated carrier concentration is expressed as an areal density d_h. Note that d_h is proportional to n_i for both cases. Current in the field-free bulk is driven by the carrier gradient $\mathrm{d}n/\mathrm{d}x$. For constant D, the profile is linear and J is proportional to n_i. However for a concentration dependant D, the profile will be curved such that $D\mathrm{d}n/\mathrm{d}x$ remains constant.

Additionally, for most functional forms of concentration dependent D, d_h will still be proportional to n_i.[104]

3.3.2. Experimental Results

In order to demonstrate the phenomenon of EE-SCLC experimentally, thin films of a conjugated polyelectrolyte were deposited on p-type silicon substrates. The conjugated polyelectrolyte, PA_C, is a cationically functionalized polyacetylene with electrochemically stabile counter-ions[93] (see Figure 2.1). The top electrode in

these structures is evaporated gold. Unlike previously studied[104] structures with symmetric gold electrodes (Figure 3.5b), the samples on silicon substrates display significant current rectification (Figure 3.5a).

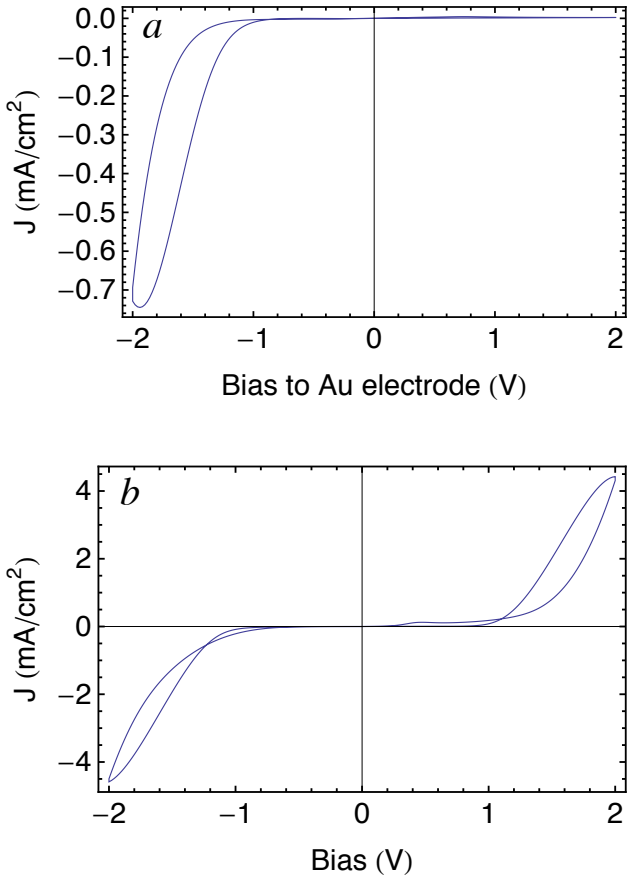

Figure 3.5. J-V curves for Au/PA_C/p-type Si system (a) and a Au/PA_C/Au system (b). The reported bias is that applied to the Au electrode, the convention for all following measurements. Note the current rectification for the former case, the sign of which is consistent with the EE-SCLC model for a hole-conducting system.

The hysteresis evident in these plots is characteristic of the slow response of the mobile ions to the applied bias[24]. Comparing to the Au/ Si /Au system, it is evident that the rectification observed for p-type Si / PA_C / Au originates from the

suppression of current when positive bias is applied to the Au electrode. This is notable because positive bias, where little current is observed, corresponds to hole injection from the gold electrode, even though the suitability of gold as a hole-injecting electrode for the material PA_C has been established in previous work[104]. In the case of the previously examined Au / PA_C / Au system, JV sweeps are symmetric, but otherwise resemble the behavior of the p-type Si / PA_C / Au structure under forward bias. Furthermore, by exposing biased PA_C thin films to ammonia vapor, it has been demonstrated that below 1.4 V applied bias Au electrodes inject holes, as would be expected from its work function relative to polyacetylene valence band. It may thus be concluded that suppression of current observed when positive bias is applied to the gold electrode may instead be attributed to the extracting silicon electrode.

Qualitatively, this matches with the model described above. However, the time-dependant response of mobile ions evident in Figure 3.5a interferes with a more quantitative comparison, suggesting that more time for equilibration is required. Additionally, we expect that the general model described above will not accurately describe the current density of our system, due to a concentration-dependant diffusion coefficient of carriers in the material PA_C. In equation 1 of the above model, it is assumed that the *D* is constant, however previously published characterization of PA_C reveals that this is not the case, and that *D* exhibits a power-law dependence on the carrier concentration, consistent with the hopping transport often observed in disordered organic semiconductors.

In the instance of a concentration-dependant diffusion coefficient, a more direct comparison with the predictions of the model may be achieved by measuring the density of injected electronic charge. The total electronic carrier density d_h (carriers/cm^2) was measured using NIR absorbance at 1310nm. This is possible because injected charge in polyacetylene take the form of solitons, which exhibit a broad NIR absorbance[78,79] extending beyond the band edge of the silicon substrate (the gold electrode is thin enough to be semi-transparent). A more extensive characterization of this technique has been previously published for this material.[104]

NIR absorbance was used to quantify injected carrier density over the course of a very slow voltage sweep of 2mV/min, in order to study the near steady-state behavior of the system. This sweep rate was validated by examining the approach to steady state during a 1V potentiostatic measurement (Figures 3.6a and b). The RC time constant extracted from the charging is 390 s, corresponding to a cutoff frequency of 4×10^{-4} Hz. The 1.4V 2mv/min sweep, expressed as a frequency, would correspond to $\sim6\times10^{-6}$ Hz.

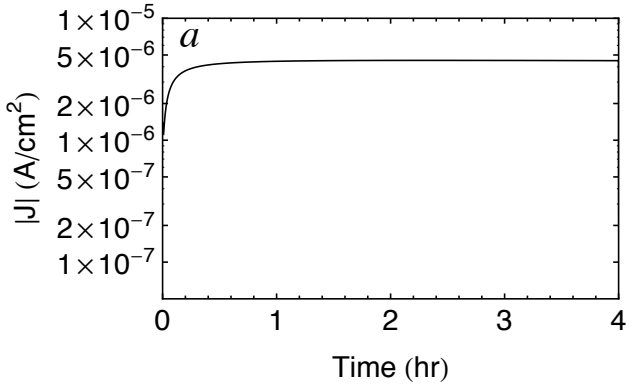

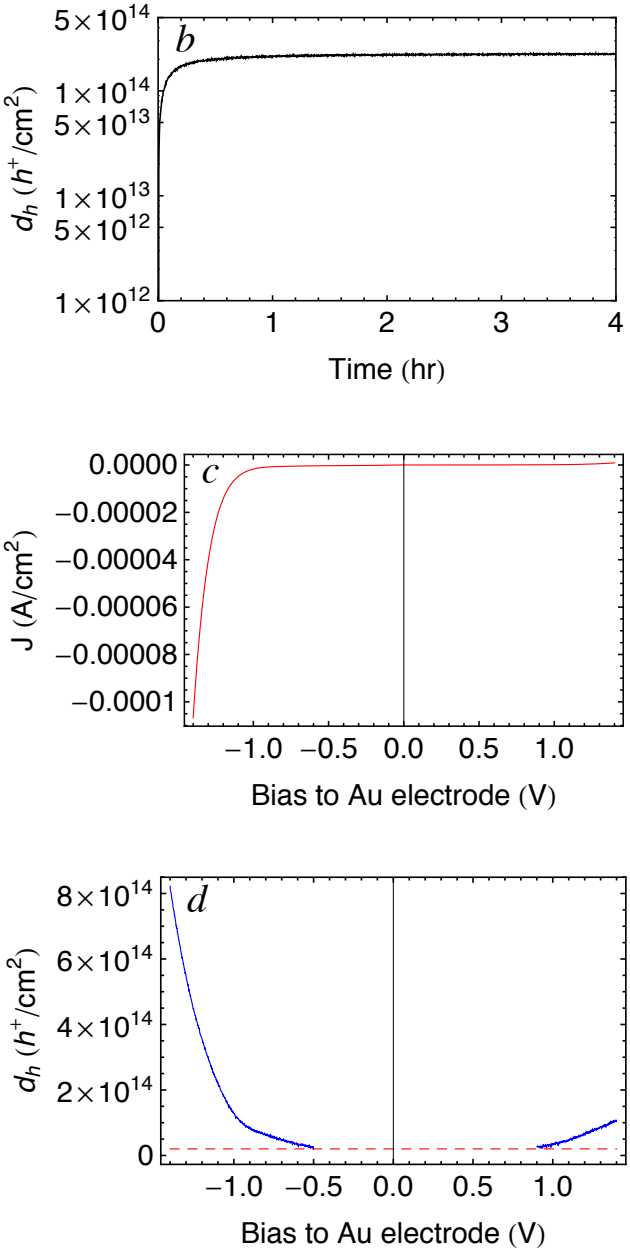

Figure 3.6. Current and carrier density over the course of 4 hours of constant -1V applied bias (a and b). Current and carrier density for a very slow voltage sweep of 2mV/min are shown, from 1.4V to -1.4V (c and d). Below a carrier density of 2×10^{13} h^+/cm^2 (- - -), the absorbance change is insufficient for carrier quantification.

The current and injected carrier density from the slow voltage sweep are shown in Figures 3.6c and d. As expected based on the concentration-dependant diffusion

coefficient, asymmetry in J with applied bias was greater than the asymmetry in d_h. Below ~2×10^{13} carriers/cm^2, there was insufficient injection to quantify via absorbance. The d_h values from the voltage sweep were then compared to predictions from the above EE-SCLC model articulated above (Figure 3.7). Specifically, equations 2 and 3 in conjunction with equations 18-22 were used to calculate n_i. Both the d_h and n_i values were normalized to their respective magnitudes at V_{app} = -1.4V. It is appropriate to compare d_h and n_i values because they are proportional to one another, even for a D which displays a power-law dependence on concentration[104] (see Figure 3.4).

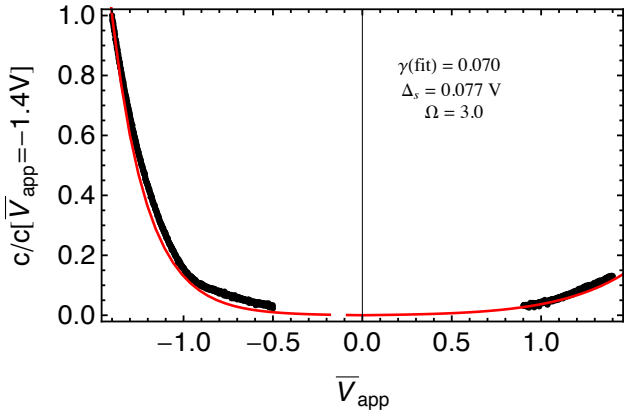

Figure 3.7. Comparison of experimentally determined d_h (black) to the predicted n_i from the EE-SCLC model (red), both normalized to V_{app} = -1.4V. Even in the case of an n dependant D, d_h is expected to be proportional to n_i (see Figure 3.4). The values of Ω and Δ_s in this system are measured experimentally, while the value of γ is fit.

By fitting a single parameter, γ, the scaling of charge injection in the EE-SCLC model was shown to exhibit a close correlation with the experimental data. A more detailed explanation of the other parameters involved in this model, which have been separately determined, is discussed below.

3.4. Discussion

Wherever MIEC's are interfaced with semiconducting materials of similar or lesser capacitance, EE-SCLC will become relevant to understanding current-voltage and charge-voltage behavior. The phenomenon will limit carrier injection (relative to metal electrodes), and injection will be most strongly limited when the semiconductor is used as the extracting electrode, resulting in rectification. When the semiconductor functions as the extracting electrode, space charge in the semiconductor will limit charge injection. This is similar to the conventional space-charge-limited current (SCLC) model,[88] except that in this case the space charge is localized not in the current-limiting conductor but in an adjacent electrode.

Three separate parameters of the system must be considered in order to predict its behavior in accordance with the EE-SCLC model. The most important of these in determining the rectification is γ, which relates the capacitance of the MIEC with that of the semiconductor under accumulation (see equation 17). The larger the value of γ, the greater the current asymmetry. As demonstrated in Figure 3.3, significant current asymmetry emerges when the value of γ is still below 1, which is to say that an MIEC capacitance approaching that of the semiconductor under accumulation is sufficient for strong EE-SCLC behavior.

The value of γ may be calculated so long as the dielectric constant and dopant / mobile ion densities of the semiconductor / MIEC are known. In the case of PA_C, the mobile ion density c_o is unknown so γ must be fit (see Figure 3.7). The

value of c_o calculated from the fit γ is 7×10^{16} cm^{-3}. While this is a small fraction of the total ion density (1.8×10^{21} cm^{-3}) in PA_C, the effective density of mobile ions is estimated to be much lower[24], and to decrease dramatically when residual solvent is baked out of the material. This is likely related strong ion pairing in the low-dielectric medium and to the morphology of the polymer, in particular the amount of interstitial space in which the bulky organic anions may be conducted. Note that the calculation of c_o as described above relies on the Guoy-Chapman model of ion polarization in the MIEC, but the EE-SCLC model as presented does not implicitly require this, so long as capacitance in the MIEC is voltage-independent. Ultimately, determination of γ in a system only requires knowledge of the capacitance of the MIEC and semiconductor under depletion and accumulation.

The relation between applied voltage and injected electronic carriers is also strongly influenced by the material parameter Ω, which determines how electronic carrier concentration depends on the potential drop across the MIEC diffuse layer. A large value of Ω functions to suppress exponential increase in injected charge with applied bias, expanding the characteristic behavior of the system over a larger bias range. This parameter may be experimentally determined for the MIEC material by cyclic voltammetry. In the case of PA_C, Ω was found to have a value of 3.0[93,104].

Finally, accurate prediction of *J-V* or *Q-V* behavior using the EE-SCLC model requires knowledge of Δ_s, the Fermi level offset between the MIEC and semiconductor. This offset shifts the voltage separating semiconductor accumulation and depletion away from $V_{app} = 0$, and subtly modifies the resulting *J-V*

curve. The value of the MIEC Fermi level may also be experimentally estimated through measurement of its electrode potential. In the case of PA_C, Δ_s was determined to have a value of 0.077 V.[104] The Fermi level offset between the MIEC and metal does not need to be accounted for, as the capacitance of the MIEC at the metal electrode is voltage-independent. In practical application of the EE-SCLC model, calculations may be significantly simplified if the Fermi level of the MIEC and semiconductor are sufficiently similar, which they often will be for rationally chosen MIEC/electrode pairs (see equations 23 and 24).

As described above, knowledge of the parameters γ, Ω, and Δ_s ultimately enable us to anticipate the voltage dependence of n_i and n_e, the carrier concentrations in the MIEC at the electrode interfaces (absolute values for n_i and n_e require knowledge of the intrinsic carrier concentration n_0). However, it should be noted that *J-V* behavior will still depend on the diffusion coefficient of electronic carriers in the MIEC. If D may be reasonably assigned a single value, then J will be proportional to the anticipated n_i, and may be calculated as per equation 1. However, if the value of D displays a dependence on electronic carrier concentration, then this will result in a nonlinear dependence of J on n_i. Calculating J then depends on the functional form of D. For instance, for a diffusion coefficient which has the form $D = An^B$, the resulting current will be proportional to n^{B-1}.[104] It should also be noted that concentration dependent diffusion coefficients, so long as the coefficient varies positively as a function of concentration, will invariably magnify injection asymmetry in the observed current. (see Figure 3.6c and d).

Accurate prediction of J thus relies on knowing the electronic parameters of the MIEC, including D. However, D may be experimentally determined by methods similar to those described above. If Ω is known (for instance from cyclic voltammetry), then the functional form of D may be determined from J-V behavior. If n_0 is also known, then the value of D may likewise be determined. These calculations are simplified for systems with two metal electrodes (γ, $\Delta_s \approx 0$). However, if these parameters are not known, then calculation of D requires a separate measurement of injected carrier density d_h (note that injected electronic carriers are present throughout the length of the MIEC and are distinct from ionic charge regions Q_1 and Q_2). There are various approaches to obtain this value: ideally it can be determined through direct measurement as described above. Electronic measurements, for instance short circuit discharge current following fixed bias, offer alternate methods,[34] although these are subject to interfering factors such as internal charge recombination.[104]

The above discussion may primarily demonstrate just how complex it can be to can accurately predict J purely from material parameters. However, the difficulty of this task should also serve as a warning against making detailed analysis of an experimental systems based solely on electrical measurements. Particularly in organic semiconductors, concentration dependent diffusion coefficients/mobilities are common, and can have a powerful influence over observed behavior. If possible, measurement of injected carriers often provides a more direct route as to the governing behavior of a system. Finally, the unexpected nature of the behavior described above commends us to avoid analyzing the individual components, and

even interfaces, of an experimental system in isolation. Particularly when MIEC's are present, electronic charge may be coupled in unanticipated ways between different parts of a system.

3.5. Conclusion

We have developed a model that explains and quantitatively predicts previously unexpected rectifying behavior when MIEC's are interfaced with semiconducting contacts. We have corroborated this model in an experimental system comprised of a hole-conducting polyacetylene-based MIEC contacted with gold and p-type Silicon. In this system we observe a current asymmetry greater than 100X, favoring hole injection from the silicon electrode. Our model, designated extracting-electrode space-charge limited current (EE-SCLC) describes how this behavior results from the limited capacity of a semiconducting contact to support space charge when pushed into depletion. Unexpectedly, for an MIEC chosen to make an Ohmic contact to the semiconductor (roughly matching the Fermi levels), the semiconductor exerts this current-limiting behavior when it functions as the *extracting* electrode. Whether or not a metal/MIEC/semiconductor system will display this behavior may be predicted primarily from γ, a term which relates the capacitance of the MIEC with that of the semiconductor under accumulation. If the MIEC capacitance approaches that of the semiconductor, then a substantial fraction of applied bias will be dropped across the semiconductor, particularly when it

functions as the extracting electrode (leading to current asymmetry). This phenomenon may govern device behavior in various applications where MIEC's are interfaced with other semiconductors, such as injection layers for perovskite cells and OPV's, electrolyte-gated transistors, and polymer light-emitting electrochemical cells.

3.6. Bridge to Chapter IV

Chapter III demonstrates the importance of carefully considering the interactions of an MIEC with adjacent materials. It shows how expectations of device function based purely on consideration of the *electronic* system will often prove wrong when one of the materials is an MIEC. As the EE-SCLC phenomenon demonstrates, when MIEC's are present electronic charge may be coupled in unanticipated ways between different parts of a system. Chapter III addressed these interactions between MIEC materials and ion-blocking semiconductors. As chapter IV will demonstrate, a different set of interactions can dominate the behavior of MIEC materials when they are contacted to ion-*conducting* semiconductors. A contact between two different MIEC's with very similar electronic systems but asymmetric ionic systems will demonstrate the importance of these considerations. Specifically, the interface between materials with different signs of mobile ions will be shown to stimulate a photovoltaic effect, and the iterative interactions between the ionic and electronic systems as they subsequently

equilibrate to illumination will be explored. Again, NIR absorbance will prove a useful tool for revealing hidden dynamics.

CHAPTER IV

PHOTOCHEMICAL DOPING OF AN ADAPTIVE MIX-CONDUCTING P-N JUNCTION

This chapter is a rewritten and reformatted version of Lin, F., Walker, E. M. & Lonergan, M. C. J. Phys. Chem. Lett. 1, 720–723 (2010) The experiments were performed on a device structure fabricated by Fuding Lin, who also collected the data shown in Figure 4.2. The remaining data was collected by Fuding and myself together, on an experimental system assembled by me. Mark Lonergan provided helpful discussion and editorial guidance.

4.1. Introduction

Mixed ionic-electronic conductors (MIEC's) have found increasing application in a number of different device structures. These include light-emitting electrochemical cells (PLEC),[34] electrolyte gated transistors,[37,38] and electrochromics.[41] MIEC systems have also been utilization in photovoltaics, in the

form of dye-sensitized solar cells (DSC), also known as Gratzel cells.[105] DSC's represent a unique application of the MIEC system; ionic and electronic conduction occurs in separate phases, and while this is sometimes the case in other MIEC systems, DSC's display an additional level of segregation between electron and hole conduction systems. The electron-conducting TiO_2 network exists in sufficiently intimate contact with the electrolyte for electronic space charge to be ionically compensated, but the TiO_2 itself does not function as ionic conductor. In this sense, a DSC represents a junction between an electrically insulting ion conductor and a distinct ion-blocking electron conductor. As a result, the role of ionic asymmetry in photovoltaic MIEC systems has gone largely unexplored.

Many MIEC systems function as solid electrolytes, effectively conducting both signs of ion. However, there have also been investigations of materials functionalized with ions so that only one sign of ion is mobile.[87] When two oppositely functionalized materials are interfaced, a junction of differential ion mobility is formed, which may be termed a hetero-ionic junction. [75] Only recently have these systems attracted attention for their potential application to photovoltaics. In particular, a junction of ionically functionalized organic semiconductors $DPAS^- Na^+/[Ru(bpy)_3]^{2+}(PF_6)^-_2$ was investigated by Bernards et al. as a PLEC and photovoltaic system[106]. The potential for ion migration-induced built-in voltage was acknowledged in this work, but interpretation was complicated by the fact that the constituents of the heterojunction had a substantial frontier orbital offset (~0.7 V). In this work we analyze the photovoltaic behavior of a more

symmetric MIEC junction with little or no orbital energy offset, in order to isolate the influence of ionic asymmetry on a photovoltaic system.

4.2. Experimental

Polyacetylene ionomers were synthesized using the ring- opening metathesis polymerization of ionically functionalized cyclooctatetraenes described in a previous study.[87] The Au|PA_A|PA_C|Au samples were fabricated by first evaporating the bottom electrode on clean glass substrates, followed by sequential spin-coating of PA_C and PA_A out of DMF and methanol solutions, respectively, and they were completed by thermal evaporation of the top Au contact. Both electrodes were 15nm thick. A Keithley 236 Source-Measure Unit in combination with an Agilent 4156C parameter analyzer was used for photoresponse measurements. The light source used for photovoltaic response experiments was either a 30 mW green diode laser at λ=532 nm with a beam size of about 1 mm or a tunable 5 W diode-pumped solid-state laser from Coherent, Inc., with an expanded beam size of around 1 cm. The change in electronic carrier density during the sample's response to green laser illumination was monitored through the change in the absorption of a weak NIR beam at λ = 1305 nm. All measurements were carried out with the sample under an active vacuum of better than 20 mTorr.

4.3. Results

The photovoltaic response of a hetero-ionic MIEC junction was explored by simultaneously illuminating it from both sides with ~200 mW/cm^2 of green light (see Figure 4.1).

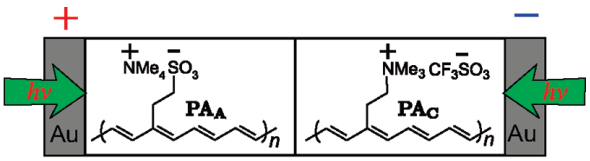

Figure 4.1. A hetero-ionic junction composed of anionically (PA_A) and cationically (PA_C) functionalized polyacetylene layers, sandwiched between two gold electrodes. Electrodes are sufficiently thin to enable illumination from both sides.

This geometry of illumination was used to minimize the observed effects of any hetero-junctions present at either of the gold-polymer interfaces. The 532 nm laser is near the absorbance maximum of the functionalized polyacetylenes used to construct the junction. Over an exposure period of 15 minutes, the open-circuit voltage (V_{OC}) and the short-circuit current density (J_{SC}) were collected in two separate measurements (see Figure 4.2).

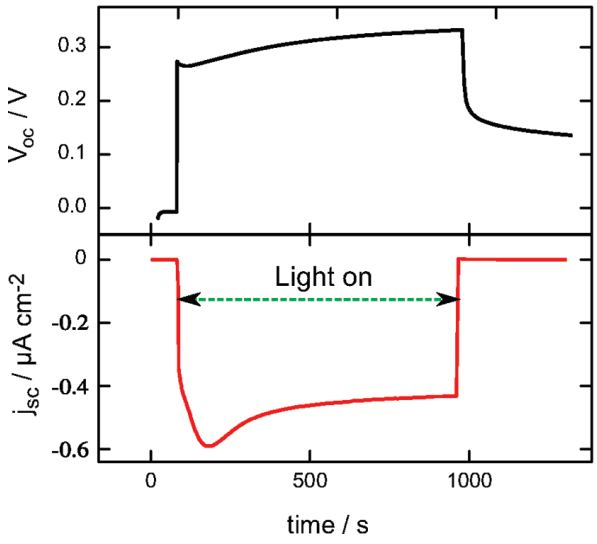

Figure 4.2. V_{OC} and J_{SC} in response to symmetric illumination with a 200mW/cm^2 green laser.

Two components or the V_{OC} and J_{SC} transients are visible: an instantaneous response to illumination and a slower subsequent evolution. While the J_{SC} drops to zero when the illumination ceases, the V_{OC} retains a significant residual value that decays very slowly. The intensity of the response contrasts with that of individual PA_C or PA_A films in similar conditions, which only display a V_{OC} of ~10mV.

In order to observe the evolution of electronic charge carrier density as a result of illumination, the MIEC heterojunction was exposed to a 30 mW green laser, this time only on a single side (illuminating from PA_C). Concurrently, the absorbance in the NIR at 1305 nm was measured in order to probe the density of electronic carriers present in the device[104]. It should be noted that this measurement registers a *change* in carrier density but not the absolute value. As with the previous measurement, the onset of illumination was recorded. However

in this measurement, over the course of a single illumination the film was alternated between open and short circuit with a frequency of 4 min (see Figure 4.3).

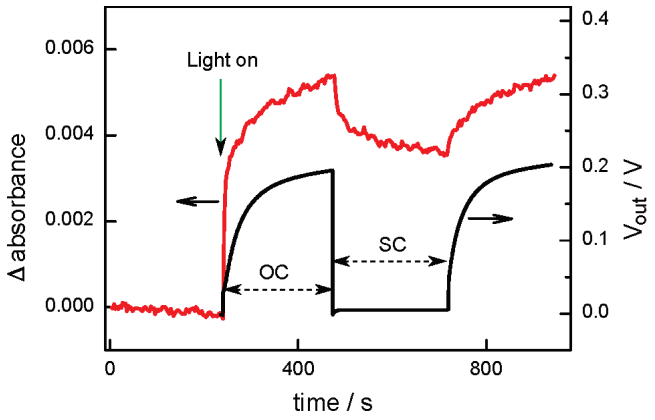

Figure 4.3. Absorbance change at 1305 nm and V_{OC} in response to illumination with a 30 mW green laser. After illumination, the electrode contacts of the junction were alternately placed under open circuit and short circuit.

The voltage response is shown along with the NIR absorbance change. The absorbance displays two components: an instantaneous response to illumination and a longer evolution which mirrors the rise in V_{OC}. When the junction is subject to short circuit, the absorbance decays on a similar timescale. Identical measurements were performed on single-layer films of PA_C and PA_A (see Figure 4.4), which displayed the instantaneous response in absorbance, but no response whatsoever to the alteration of open/short circuit.

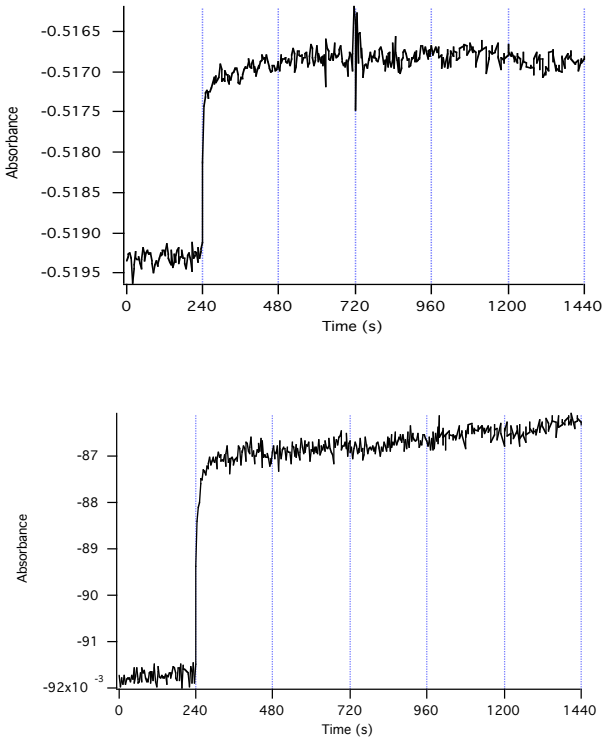

Figure 4.4. Absorbance at 1305 nm in response to illumination for PA_C (top) and PA_A (bottom) single layers. As with the junction in Figure 4.3, the films are alternately switched between open and short circuit, this time with no response.

4.4. Discussion

Interpreting the bilayer measurements detailed above, it is useful to note that J_{SC}, V_{OC}, and NIR ΔAbsorbance (representing electronic carrier density) all display both instantaneous and long-term components in their response to illumination. In comparison, single-layer films of PA_C or PA_A exhibit negligible V_{OC} or J_{SC}, although they do show the instantaneous component of the ΔAbsorbance response. The immediate jump in electronic carrier density is expected in both

single-layer and bilayer systems as a result of photogenerated charge carriers. The instantaneous values of V_{OC} and I_{SC}, on the other hand, require some source of asymmetry in the electronic system at the moment of illumination. A band offset between PA_C and PA_A materials could conceivably explain this result. However, the materials PA_C and PA_A were intentionally formulated to have similar electronic structures, and electrochemical[93] and optical[87] measurements indicate frontier orbital positions which differ within 0.05 V. For intrinsic semiconductors the minimum band offset sufficient to explain the instantaneous V_{OC} observed in Figure 4.2 would be 0.27 V.

If the heterojunction model of a conventional OPV is insufficient to explain the observations, there is an alternate interpretation which might describe both the magnitude of the instantaneous response, as well as the long-term evolution observed in J_{SC}, V_{OC}, and electronic carrier density. While the electronic systems of this junction are expected to be quite symmetric, the *ionic* system is not. Both materials possess a similar density of ions, but in PA_C the cations are immobile and in PA_A the anions, each with the opposite ion mobile. In this sense a PA_C/PA_A junction is the ionic analog of a conventional p-n junction. It would be expected that the disparity in ion concentration n_{A^-} or n_{C^+} across the junction would lead to diffusion, resulting in uncompensated charge in each material. Equilibrium would be reached once the emerging electric field was sufficient to level the chemical potential of ions (μ_{A^-} or μ_{C^+}) across the junction (see Figure 4.5a). This would result in a built-in potential ϕ_{bi}.

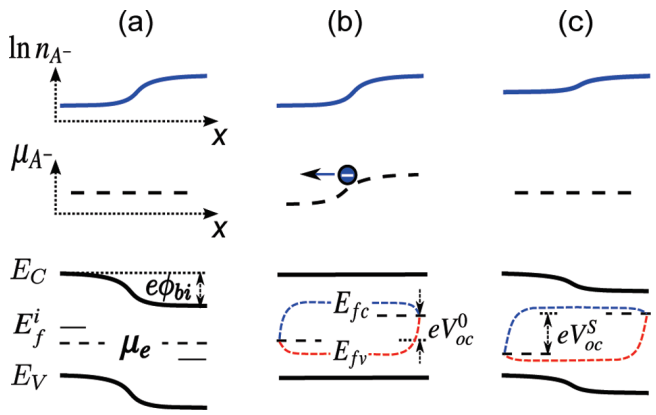

Figure 4.5. Mobile anion concentration (n_{A^-}), anion electrochemical potential (μ_{A^-}), and band bending diagrams across the width of the junction in three cases: following equilibration in the dark (a), immediately upon illumination (b), and equilibrated to illumination (c).

Electronic carriers must also be part of this equilibrium. For a junction of intrinsic materials in the dark, the concentration of free electronic carriers will be too low to radically alter the potential picture. However, this can change when a significant quantity of photogenerated carriers are introduced (Figure 4.5b). Upon illumination the increased population of carriers in both bands splits the Fermi level into valence and conduction band quasi-Fermi levels E_{fv} and E_{fc}, enabling the generation of photocurrent. Additionally, these photogenerated carriers may now screen ϕ_{bi}, with two significant consequences. The first is that some fraction of ϕ_{bi} may now be registered as an open-circuit voltage across the symmetric electrode contacts (V^0_{OC}). Second, screening of the ionic-space charge neutralizes the field which had been holding diffusion of ions in check. A chemical potential gradient for the ions is restored, and they respond with renewed diffusion. However, unlike the initial dark equilibration, there is now a significant concentration of electronic

carriers and a motive force to shuttle them across the junction. Ions diffusing across the junction may now be compensated by an opposite flow of electronic carriers. This process constitutes a photochemical self-doping of the MIEC junction, such that the PA_C layer would be n-doped and the PA_A layer p-doped. Increasing doping would be registered in the open-circuit voltage as the Fermi level in PA_A and PA_C are driven farther apart. Eventually a new equilibrium will develop where doping has reached its maximum extent, and the diminished gradient of ions across the junction is held in check by a decreased internal field (Figure 4.5c).

The model described above explains how a hetero-ionic junction with no initial band offset could display a substantial photovoltage. It also makes several other key predictions. Firstly, the V_{OC} would be expected to rise with increasing time under illumination, and the timescale of this rise would be consistent with that of ionic redistribution in the constituent MIEC materials. Indeed, the timescale of the observed V_{OC} rise conforms with the ionic response time observed through impedance and potentiostatic measurements[24,104]. This model also predicts that V_{OC} increase would be accompanied by a rise in electronic carrier density, as was observed by NIR absorbance. Finally, it is anticipated that short-circuiting an illuminated junction would drain a significant fraction of the accumulated carriers (although a junction equilibrated at short circuit would retain some doping in order to drive J_{SC} to the electrode contacts).

The only observation not explicitly predicted by the photochemical self-doping model is the evolution of J_{SC} following illumination. J_{SC} displays an initial rise,

a peak, and then decay to steady-state somewhat above the instantaneous value. However, the expected evolution of J_{SC} based on this model is not as clear as V_{OC}. Additionally, it is known that doping in organic semiconductors is often accompanied by higher rates of recombination, which will suppress the generation of photocurrent.

The available evidence, including the absence of photovoltaic activity or long-term evolution of carrier population in the corresponding single layer systems, supports the assertion that the observed photovoltaic response is tied to the exchange of ions across the junction. This interpretation is strengthened, and the analysis simplified, by the similarity of the PA_C and PA_A polymers, particularly with regards to their electronic systems. This uniformity, when contrasted with the strong asymmetry implied by the initial V_{OC} value, enables us to focus on the contribution of *ionic* asymmetry to this photovoltaic system. These results indicate a dark $\phi_{bi} > 0.27$ V, with ionic diffusion as the only apparent source. Illumination is shown to increase both the potential across the junction and its carrier density in a manner consistent with photochemical self-doping.

It is tempting to use the NIR absorbance measurements as the basis of a direct quantification of carriers/cm^2, as previously published[104]. These values which would assist in building a more comprehensive model of this system. However, calibration of this measurement would be difficult, as the system contains two different types polymers and two different signs of carrier, each of which might

have a different extinction coefficient. In this case, precise quantification would only be possible with an assumption of internal charge balance, which may not be valid.

The demonstration of a photovoltaic effect originating from ionic asymmetry suggests the potential for improvement of conventional OPV structures. The relative absence of p-n diode type structures in OPV applications is partly owed to the difficulty of maintaining such structures against un-doping by dopant diffusion. Interestingly, this photovoltaic system relies on a p-n diode like structure *formed* by ion diffusion. The photochemical self-doping process might also be usefully applied in its ability to neutralize current-limiting space charge near the interface. The evolution of J_{SC} observed suggests that higher levels of doping may ultimately be counterproductive, which could be addressed by judiciously limiting ion density. It should also be noted from a practical standpoint that only one of the materials in the junction needs to be a fixed/mobile MIEC in order to display this effect, so long as the other material is not ion blocking. Separate from OPV applications, one could imagine other uses for a system which can vary doping levels and drive ion motion with illumination.

4.5. Conclusion

We have observed a photovoltaic effect in a hetero-ionic MIEC junction, and we have demonstrated how this effect originates from an ion-diffusion process

analogous to the equilibration of a conventional p-n junction. We further demonstrate a previously undescribed effect whereby an ionic junction can interact with photoexcited carriers to drive further ion diffusion, compensated by photochemical doping of the constituent MIEC materials. Our conclusions are supported by the evolution of illuminated V_{OC} and NIR absorbance on a timescale consistent with ion redistribution. This process offers the potential for improving OPV efficiency as well as developing entirely new applications.

CHAPTER V

CONCLUDING SUMMARY

The complex and mutually interdependent ionic and electronic systems of MIEC's present a significant challenge to characterization efforts. Both quantitative and qualitative understandings of the internal dynamics are confounded by the convolution of these systems. However, the use of NIR absorbance has proved very valuable by providing a separate measurement of injected electronic carrier density. While this single parameter does not provide a complete picture, carefully combining this measurement with more conventional techniques enables us to draw important conclusions about systems that would otherwise be opaque.

Specifically, it has been demonstrated that the technique can be used to quantify carrier mobility, a parameter that has generally not been measurable in MIEC systems. In the functionalized polyacetylene studied, carrier mobility was shown to exhibit a power-law concentration dependence in the injection regime relevant to MIEC conduction, a detail which would have been missed if mobility had been measured by operating outside the timescale of ion motion.

We further show that NIR absorbance, together with a more comprehensive model of charge injection and transport, can help to elucidate some of the more obscure and unintelligible behavior of MIEC's. An unexamined and potentially important dynamic for MIEC charge injection materials is explored, wherein injection is limited by the capacity of the extracting electrode material to support space charge. This dynamic is described by a quantitative model dubbed extracting-electrode space-charge limited current (EE-SCLC), and experimentally demonstrated using a p-type Si contact. Novel dynamics are also demonstrated in the contact between two MIEC's with dissimilar ion mobility. In this case the junction displays a photovoltaic effect where none would be expected based on the electronic system alone. The mechanism behind this effect is shown to result from ion diffusion between the materials, and a similar process enables the MIEC junction to photochemically self-dope in response to illumination, driving up the built-in potential between the MIEC layers.

More broadly, two major conclusions are drawn. Firstly, the electronic measurements used to characterize semiconducting systems are insufficient when applied to MIEC systems; additional lines of evidence are needed. Secondly, the interaction of MIEC materials with the other elements in a device structure must be carefully considered on both the electronic and ionic level. Mobile ions may display significant and unanticipated effects beyond enhanced charge injection.

APPENDIX

SUPPORTING INFORMATION TO CHAPTER II

Calculation of expected carrier density in a two electrode system with electrochemically-supported charge injection.

This calculation is based on the integrated current from cyclic voltammetry of a thin film of the conjugated ionomer PA_C, shown in Figure 2.5. The expected carrier density d_h is obtained by Eq. 3:

$$qd_h^{EC} = \eta Q_{CV}(E)$$

where $Q_{CV}(E)$ is the integrated current from the CV as a function of electrode potential. The factor η is defined as follows:

$$\eta = \frac{L}{1.44 V_{CV}}$$

where L is the thickness of the two-electrode film used in the primary experiment and V_{CV} is the volume of material used in the CV. The factor of 1.44 is used to compensate for the non-uniform distribution of charge in the two-electrode case as opposed to the CV film (see Figure 2.11). With the concentration at the injecting

electrode n_h(E) determined by the charge concentration from the CV, the factor 1.44 can be obtained from Eq. 12 as:

$$\left(\frac{\gamma+2}{\gamma+1}\right)$$

where γ is the power dependence of the diffusion coefficient on concentration. This assumes the high-injection limit of transport where the factor α is negligible, and thus the first three points (0.5, 0.6, and 0.7 V) can be expected to deviate slightly from the trend.

REFERENCES CITED

1. Chiang, C. K. *et al.* Electrical conductivity in doped polyacetylene. *Phys. Rev. Lett.* **39,** 1098–1101 (1977).

2. Burgués-Ceballos, I., Stella, M., Lacharmoise, P. & Martínez-Ferrero, E. Materials Chemistry A. *J. Mater. Chem. A* **2,** 17711–17722 (2014).

3. Chang, Y.-F. *et al.* Organic Electronics. *Organic Electronics* **13,** 2149–2155 (2012).

4. Kawase, T., Shimoda, T., Newsome, C., Sirringhaus, H. & Friend, R. H. Inkjet printing of polymer thin film transistors. *Thin Solid Films* **438-439,** 279–287 (2003).

5. Wang, Z. *et al.* Esterification of Indoline-Based Small-Molecule Donors for Efficient Co-evaporated Organic Photovoltaics. *J. Phys. Chem. C* **118,** 14785–14794 (2014).

6. Logothetidis, S. & Laskarakis, A. Towards the optimization of materials and processes for flexible organic electronics devices. *Eur. Phys. J. Appl. Phys.* **46,** 12502 (2009).

7. Weinberger, B. R., Akhtar, M. & Gau, S. C. Polyacetylene photovoltaic devices. *Synthetic Metals* **4,** 187–197 (1982).

8. Spanggaard, H. & Krebs, F. C. A brief history of the development of organic and polymeric photovoltaics. *Solar Energy Materials and Solar Cells* **83,** 125–146 (2004).

9. Wang, J. *et al.* Journal of Photochemistry and Photobiology C: Photochemistry Reviews. *'Journal of Photochemistry & Photobiology, C: Photochemistry Reviews'* **17,** 69–104 (2013).

10. Boix, P. P., Nonomura, K., Mathews, N. & Mhaisalkar, S. G. Current progress and future perspectives for organic/inorganic perovskite solar cells. *Materials Today* **17,** 16–23 (2014).

11. Tolbert, L. M. Solitons in a box: the organic chemistry of electrically conducting polyenes. *Acc. Chem. Res.* **25,** 561–568 (1992).

12. Boudreaux, D. S., Chance, R. R., Bredas, J. L. & Silbey, R. Solitons and polarons in polyacetylene: Self-consistent-field calculations of the effect of neutral and charged defects on molecular geometry. *Phys. Rev. B* **28,** 6927 (1983).

13. Kivelson, S. & Wu, W. Photoproduction of neutral soliton pairs in trans-(CH)x. *Phys. Rev., B Condens. Matter* **34,** 5423–5429 (1986).

14. Arkhipov, V. I. & Bässler, H. Exciton dissociation and charge photogeneration in pristine and doped conjugated polymers. *phys. stat. sol. (a)* **201,** 1152–1187 (2004).

15. Piris, J. *et al.* Photogeneration and Ultrafast Dynamics of Excitons and Charges in P3HT/PCBM Blends. *J. Phys. Chem. C* **113,** 14500–14506 (2009).

16. Snedden, E. W., Monkman, A. P. & Dias, F. B. Photophysics of Charge Generation in Organic Photovoltaic Materials: Kinetic Studies of Geminate and Free Polarons in a Model Donor/Acceptor System. *J. Phys. Chem. C* **116,** 86–97 (2012).

17. Coffey, D. C. *et al.* An Optimal Driving Force for Converting Excitons into Free Carriers in Excitonic Solar Cells. *J. Phys. Chem. C* **116,** 8916–8923 (2012).

18. Yost, S. R. & Van Voorhis, T. Electrostatic Effects at Organic Semiconductor Interfaces: A Mechanism for 'Cold' Exciton Breakup. *J. Phys. Chem. C* **117,** 5617–5625 (2013).

19. Kendrick, M. J. *et al.* Formation of the Donor–Acceptor Charge-Transfer Exciton and Its Contribution to Charge Photogeneration and Recombination in Small-Molecule Bulk Heterojunctions. *J. Phys. Chem. C* **116,** 18108–18116 (2012).

20. Gélinas, S. *et al.* The Binding Energy of Charge-Transfer Excitons Localized at Polymeric Semiconductor Heterojunctions. *J. Phys. Chem. C* **115,** 7114–7119 (2011).

21. Chung, T. C., Moraes, F., Flood, J. D. & Heeger, A. J. Solitons at high density in trans-(CH) X: Collective transport by mobile, spinless charged solitons. *Phys. Rev., B Condens. Matter* **29,** 2341–2343 (1984).

22. Yu, G., Gao, J., Hummelen, J. C., Wudl, F. & Heeger, A. J. Polymer Photovoltaic Cells: Enhanced Efficiencies via a Network of Internal Donor-Acceptor Heterojunctions. *Science* **270,** 1789–1791 (1995).

23. Friend, R. H. *et al.* Electroluminescence in conjugated polymers. *Nature* **397,** 121–128 (1999).

24. Lin, F., Wang, Y. & Lonergan, M. Ion transport in polyacetylene ionomers. *J. Appl. Phys.* **104,** 103517 (2008).

25. Cheng, C. H. W. & Lonergan, M. C. A Conjugated Polymer pn Junction. *J. Am. Chem. Soc.* **126,** 10536–10537 (2004).

26. Groenendaal, L., Jonas, F., Freitag, D. & Pielartzik, H. Poly (3, 4-ethylenedioxythiophene) and its derivatives: past, present, and future. *Adv. Mater.* (2000).

27. Lee, M. S., Tzeng, J. S., Chen, Y. C. & Shiramatsu, T. Stability of Electrical and Photovoltaic Characteristics of HBr Solution-Doped Polyacetylene. *Jpn. J. Appl. Phys.* **28,** 1008 (1989).

28. Murphy, A. R. *et al.* Synthesis, Characterization, and Field-Effect Transistor Performance of Carboxylate-Functionalized Polythiophenes with Increased Air Stability. *Chem. Mater.* **17,** 4892–4899 (2005).

29. Weber, C. D., Robinson, S. G., Stay, D. P., Vonnegut, C. L. & Lonergan, M. C. Ionic Stabilization of the Polythiophene-Oxygen Charge-Transfer Complex. *ACS Macro Lett.* **1,** 499–503 (2012).

30. Borghini, M. C., Mastragostino, M. & Passerini, S. Electrochemical Properties of Polyethylene Oxide-Li [(CF 3 SO 2) 2 N]-Gamma-LiAlO2 Composite Polymer Electrolytes. *J. Electrochem. Soc.* (1995).

31. Bamford, D. *et al.* Ionic conductivity, glass transition, and local free volume in poly(ethylene oxide) electrolytes: Single and mixed ion conductors. *J. Chem. Phys.* **118,** 9420 (2003).

32. Fuke, N. *et al.* New Approach to Low-Cost Dye-Sensitized Solar Cells With Back Contact Electrodes. *Chem. Mater.* **20,** 4974–4979 (2008).

33. Bai, Y. *et al.* High-performance dye-sensitized solar cells based on solvent-free electrolytes produced from eutectic melts. *Nat Mater* **7,** 626–630 (2008).

34. Pei, Q., Yang, Y., Yu, G., Zhang, C. & Heeger, A. J. Polymer light-emitting electrochemical cells: In situ formation of a light-emitting pn junction. *J. Am. Chem. Soc.* **118,** 3922–3929 (1996).

35. Latini, G. *et al.* Enhanced luminescence properties of highly threaded conjugated polyelectrolytes with potassium counter-ions upon blending with poly(ethylene oxide). *J. Appl. Phys.* **107,** 124509 (2010).

36. Pei, Q., Yu, G., Zhang, C., Yang, Y. & Heeger, A. J. Polymer Light-Emitting Electrochemical Cells. *Science* **269,** 1086–1088 (1995).

37. Kim, S. H. *et al.* Electrolyte-Gated Transistors for Organic and Printed Electronics. *Adv. Mater.* **25,** 1822–1846 (2012).

38. Lin, F. & Lonergan, M. C. Gate electrode processes in an electrolyte-gated transistor: Non-Faradaically versus Faradaically coupled conductivity modulation of a polyacetylene ionomer. *Appl. Phys. Lett.* **88,** 133507 (2006).

39. Berggren, M. & Richter-Dahlfors, A. Organic Bioelectronics. *Adv. Mater.* **19,** 3201–3213 (2007).

40. Stallinga, P. & Gomes, H. L. Thin-film field-effect transistors: The effects of traps on the bias and temperature dependence of field-effect mobility, including the Meyer–Neldel rule. *Organic Electronics* **7,** 592–599 (2006).

41. Holt, A. L., Leger, J. M. & Carter, S. A. Solid-state electrochromic devices based on poly (phenylene vinylene) polymers. *Appl. Phys. Lett.* **86,** 123504 (2005).

42. Weinberger, B. R., Roxlo, C. B., Etemad, S., Baker, G. L. & Orenstein, J. Optical absorption in polyacetylene: a direct measurement using photothermal deflection spectroscopy. *Phys. Rev. Lett.* **53,** 86–89 (1984).

43. Vardeny, Z., Orenstein, J. & Baker, G. L. Photoinduced infrared activity in polyacetylene. *Phys. Rev. Lett.* (1983).

44. Yang, R. *et al.* Conjugated Oligoelectrolyte Electron Transport/Injection Layers for Organic Optoelectronic Devices. *J. Am. Chem. Soc.* **130,** 3282–3283 (2008).

45. Rosenwaks, Y., Shapira, Y. & Huppert, D. Metal reactivity effects on the surface recombination velocity at InP interfaces. *Appl. Phys. Lett.* **57,** 2552 (1990).

46. Credgington, D., Jamieson, F. C., Walker, B., Nguyen, T.-Q. & Durrant, J. R. Quantification of Geminate and Non-Geminate Recombination Losses within a Solution-Processed Small-Molecule Bulk Heterojunction Solar Cell. *Adv. Mater.* **24,** 2135–2141 (2012).

47. Reynolds, K. J., Barker, J. A., Greenham, N. C., Friend, R. H. & Frey, G. L. Inorganic solution-processed hole-injecting and electron-blocking layers in polymer light-emitting diodes. *J. Appl. Phys.* **92,** 7556 (2002).

48. Garcia, A. *et al.* Controlling Ion Motion in Polymer Light-Emitting Diodes Containing Conjugated Polyelectrolyte Electron Injection Layers. *J. Am. Chem. Soc.* **133,** 2492–2498 (2011).

49. Zhou, H. *et al.* Conductive conjugated polyelectrolyte as hole-transporting layer for organic bulk heterojunction solar cells. *Adv. Mater. Weinheim* **26,** 780–785 (2014).

50. Shen, Y., Hosseini, A. R., Wong, M. H. & Malliaras, G. G. How To Make Ohmic Contacts to Organic Semiconductors. *ChemPhysChem* **5,** 16–25 (2004).

51. Pickup, P. G. & Murray, R. W. Redox conduction in mixed-valent polymers. *J. Am. Chem. Soc.* **105,** 4510–4514 (1983).

52. Chidsey, C. E. D. & Murray, R. W. Redox capacity and direct current electron conductivity in electroactive materials. *The Journal of Physical Chemistry* **90,** 1479–1484 (1986).

53. Ambegaokar, V., Halperin, B. I. & Langer, J. S. Hopping conductivity in disordered systems. *Phys. Rev. B* **4,** 2612 (1971).

54. Arkhipov, V. I., Heremans, P., Emelianova, E. V., Adriaenssens, G. J. & Bässler, H. Weak-field carrier hopping in disordered organic semiconductors: the effects of deep traps and partly filled density-of-states distribution. *J. Phys.: Condens. Matter* **14,** 9899 (2002).

55. Peter, L. M. Characterization and Modeling of Dye-Sensitized Solar Cells. *J. Phys. Chem. C* **111,** 6601–6612 (2007).

56. deMello, J., Tessler, N., Graham, S. C. & Friend, R. H. Ionic space-charge effects in polymer light-emitting diodes. *Phys. Rev. B* **57,** 12951 (1998).

57. Manzanares, J. A., Reiss, H. & Heeger, A. J. Polymer light-emitting electrochemical cells: A theoretical study of junction formation under steady-state conditions. *J. Phys. Chem. B* **102,** 4327–4336 (1998).

58. van Reenen, S. *et al.* A Unifying Model for the Operation of Light-Emitting Electrochemical Cells. *J. Am. Chem. Soc.* **132,** 13776–13781 (2010).

59. Mills, T. J. & Lonergan, M. C. Charge injection and transport in low-mobility mixed ionic/electronic conducting systems: Regimes of behavior and limiting cases. *Phys. Rev. B* **85,** 035203 (2012).

60. An, Z. *et al.* High Electron Mobility in Room-Temperature Discotic Liquid-Crystalline Perylene Diimides. *Adv. Mater.* **17,** 2580–2583 (2005).

61. Blom, P. W. M., de Jong, M. J. M. & Vleggaar, J. J. M. Electron and hole transport in poly(p-phenylene vinylene) devices. *Appl. Phys. Lett.* **68,** 3308 (1996).

62. Campbell, A. J., Bradley, D. & Antoniadis, H. Trap-free, space-charge-limited currents in a polyfluorene copolymer using pretreated indium tin oxide as a hole injecting contact. *Synthetic Metals* **122,** 161–163 (2001).

63. Juska, G., Arlauskas, K., Viliunas, M. & Kocka, J. Extraction current transients: new method of study of charge transport in microcrystalline silicon. *Phys. Rev. Lett.* **84,** 4946–4949 (2000).

64. Hoven, C. V., Garcia, A., Bazan, G. C. & Nguyen, T.-Q. Recent Applications of Conjugated Polyelectrolytes in Optoelectronic Devices. *Adv. Mater.* **20,** 3793–3810 (2008).

65. Jiang, H., Taranekar, P., Reynolds, J. R. & Schanze, K. S. Conjugated Polyelectrolytes: Synthesis, Photophysics, and Applications. *Angew. Chem. Int. Ed.* **48,** 4300–4316 (2009).

66. Scher, H. & Montroll, E. W. Anomalous transit-time dispersion in amorphous solids. *Phys. Rev. B* **12,** 2455 (1975).

67. Kokil, A., Shiyanovskaya, I., Singer, K. D. & Weder, C. High charge carrier mobility in conjugated organometallic polymer networks. *J. Am. Chem. Soc.* **124,** 9978–9979 (2002).

68. Garcia, A., Yang, R., Jin, Y., Walker, B. & Nguyen, T.-Q. Structure-function relationships of conjugated polyelectrolyte electron injection layers in polymer light emitting diodes. *Appl. Phys. Lett.* **91,** 153502 (2007).

69. Garcia, A. & Nguyen, T. Q. Effect of Aggregation on the Optical and Charge Transport Properties of an Anionic Conjugated Polyelectrolyte. *J. Phys. Chem. C* **112,** 7054–7061 (2008).

70. Garcia, A., Brzezinski, J. Z. & Nguyen, T.-Q. Cationic Conjugated Polyelectrolyte Electron Injection Layers: Effect of Halide Counterions. *J. Phys. Chem. C* **113,** 2950–2954 (2009).

71. Garcia, A., Jin, Y., Brzezinski, J. Z. & Nguyen, T.-Q. Temperature and Electric Field Dependent Electron Transport in Cationic and Anionic Conjugated Polyelectrolytes. *J. Phys. Chem. C* **114,** 22309–22315 (2010).

72. Dimitrakopoulos, C. D. & Malenfant, P. R. L. Organic thin film transistors for large area electronics. *Adv. Mater.* **14,** 99 (2002).

73. Tanase, C., Blom, P. W. M., de Leeuw, D. M. & Meijer, E. J. Charge carrier density dependence of the hole mobility in poly(p-phenylene vinylene). *phys. stat. sol. (a)* **201,** 1236–1245 (2004).

74. Gregg, B. A. Transport in Charged Defect-Rich π-Conjugated Polymers. *J. Phys. Chem. C* **113,** 5899–5901 (2009).

75. Cheng, C. H. W., Lin, F. & Lonergan, M. C. Charge Transport in a Mixed Ionically/Electronically Conducting, Cationic, Polyacetylene Ionomer between Ion-Blocking Electrodes. *J. Phys. Chem. B* **109,** 10168–10178 (2005).

76. Kopidakis, N., Schiff, E. A., Park, N. G., van de Lagemaat, J. & Frank, A. J. Ambipolar Diffusion of Photocarriers in Electrolyte-Filled, Nanoporous TiO 2†. *J. Phys. Chem. B* **104,** 3930–3936 (2000).

77. Robinson, S. G. & Lonergan, M. C. Polyacetylene p–n Junctions with Varying Dopant Density by Polyelectrolyte-Mediated Electrochemistry. *J. Phys. Chem. C* **117,** 1600–1610 (2013).

78. Patil, A. O., Heeger, A. J. & Wudl, F. Optical properties of conducting polymers. *Chem. Rev.* **88,** 183–200 (1988).

79. Suzuki, N., Ozaki, M., Etemad, S., Heeger, A. J. & MacDiarmid, A. G. Solitons in polyacetylene: Effects of dilute doping on optical absorption spectra. *Phys. Rev. Lett.* **45,** 1209–1213 (1980).

80. Clarke, T. M., Jamieson, F. C. & Durrant, J. R. Transient Absorption Studies of Bimolecular Recombination Dynamics in Polythiophene/Fullerene Blend Films. *J. Phys. Chem. C* **113,** 20934–20941 (2009).

81. Li, Z. Q. *et al.* Infrared imaging of the nanometer-thick accumulation layer in organic field-effect transistors. *Nano Lett.* **6,** 224–228 (2006).

82. Eng, M. P., Barnes, P. R. F. & Durrant, J. R. Concentration-Dependent Hole Mobility and Recombination Coefficient in Bulk Heterojunctions Determined from Transient Absorption Spectroscopy. *J. Phys. Chem. Lett.* **1,** 3096–3100 (2010).

83. Fincher, C. R., Jr, Ozaki, M., Heeger, A. J. & MacDiarmid, A. G. Donor and acceptor states in lightly doped polyacetylene,(CH) _ {x}. *Phys. Rev. B* **19,** 4140 (1979).

84. Feldblum, A. *et al.* Opto-electrochemical spectroscopy of trans-(CH) _ {x}. *Phys. Rev. B* **26,** 815 (1982).

85. Lin, F., Walker, E. M. & Lonergan, M. C. Photochemical Doping of an Adaptive Mix-Conducting p−n Junction. *J. Phys. Chem. Lett.* **1,** 720–723 (2010).

86. Pinkerton, M. J., Le Mest, Y., Zhang, H., Watanabe, M. & Murray, R. W. Solid-state voltammetry and self-diffusion dynamics of a linear monotagged redox polymer:. omega.-ferrocenecarboxamido-. alpha.-methoxypoly (ethylene oxide). *J. Am. Chem. Soc.* **112,** 3730–3736 (1990).

87. Langsdorf, B. L., Zhou, X., Adler, D. H. & Lonergan, M. C. Synthesis and Characterization of Soluble, Ionically Functionalized Polyacetylenes. *Macromolecules* **32,** 2796–2798 (1999).

88. Lampert, M. A. Simplified theory of space-charge-limited currents in an insulator with traps. *Physical Review* **103,** 1648 (1956).

89. deMello, J. Interfacial feedback dynamics in polymer light-emitting electrochemical cells. *Phys. Rev. B* **66,** 235210 (2002).

90. Pingree, L. S. C., Rodovsky, D. B., Coffey, D. C., Bartholomew, G. P. & Ginger, D. S. Scanning Kelvin Probe Imaging of the Potential Profiles in Fixed and Dynamic Planar LECs. *J. Am. Chem. Soc.* **129,** 15903–15910 (2007).

91. Slinker, J. D. *et al.* Direct measurement of the electric-field distribution in a light-emitting electrochemical cell. *Nat Mater* **6,** 894–899 (2007).

92. Pell, W. G. & Conway, B. E. Peculiarities and requirements of asymmetric capacitor devices based on combination of capacitor and battery-type electrodes. *Journal of Power Sources* **136,** 334–345 (2004).

93. Lonergan, M. C., Cheng, C. H., Langsdorf, B. L. & Zhou, X. Electrochemical Characterization of Polyacetylene Ionomers and Polyelectrolyte-Mediated Electrochemistry toward Interfaces between Dissimilarly Doped Conjugated Polymers. *J. Am. Chem. Soc.* **124,** 690–701 (2002).

94. Lampert, M. A. & Rose, A. Volume-controlled, two-carrier currents in solids: The injected plasma case. *Physical Review* **121,** 26 (1961).

95. Buck, R. P. Electron hopping in one dimension: mixed conductor membranes. *The Journal of Physical Chemistry* **92,** 4196–4200 (1988).

96. Buda, M., Kalyuzhny, G. & Bard, A. J. Thin-Film Solid-State Electroluminescent Devices Based On Tris(2,2'-bipyridine)ruthenium(II) Complexes. *J. Am. Chem. Soc.* **124,** 6090–6098 (2002).

97. de Leeuw, D. M. Stable solutions of doped thiophene oligomers. *Synthetic Metals* **57,** 3597–3602 (1993).

98. Tanase, C., Meijer, E. J., Blom, P. W. M. & de Leeuw, D. M. Unification of the Hole Transport in Polymeric Field-Effect Transistors and Light-Emitting Diodes. *Phys. Rev. Lett.* **91,** 216601 (2003).

99. Jarrett, C. P., Friend, R. H., Brown, A. R. & de Leeuw, D. M. Field effect measurements in doped conjugated polymer films: Assessment of charge carrier mobilities. *J. Appl. Phys.* **77,** 6289 (1995).

100. Li, L., Meller, G. & Kosina, H. Analytical conductivity model for doped organic semiconductors. *J. Appl. Phys.* **101,** 033716 (2007).

101. Meyertholen, A. D. *et al.* Concentration-dependent mobility in organic field-effect transistors probed by infrared spectromicroscopy of the charge density profile. *Appl. Phys. Lett.* **90,** 222108 (2007).

102. Vissenberg, M. & Matters, M. Theory of the field-effect mobility in amorphous organic transistors. *Phys. Rev. B* **57,** 12964 (1998).

103. Edman, L., Summers, M., Buratto, S. & Heeger, A. Polymer light-emitting electrochemical cells: Doping, luminescence, and mobility. *Phys. Rev. B* **70,** 115212 (2004).

104. Walker, E. M. & Lonergan, M. C. Characterizing Charge Injection, Transport, and Mobility in a Conjugated Polyelectrolyte by NIR Absorbance. *J. Phys. Chem. C* 14929–14938 (2013).

105. O'Regan, B. & Grätzel, M. A low-cost, high-efficiency solar cell based on dye-sensitized colloidal TiO2 films. (1991).

106. Bernards, D. A., Flores-Torres, S. & Abruña, H. D. Observation of electroluminescence and photovoltaic response in ionic junctions. *Science* (2006).